LaMPlace: Learning to Optimize Cross-Stage Metrics in Macro Placement

Anonymous authors
Paper under double-blind review

Abstract

Machine learning techniques have shown great potential in enhancing macro placement, a critical stage in modern chip design. However, existing methods primarily focus on *online* optimization of *intermediate surrogate metrics* that are available at the current placement stage, rather than directly targeting the *cross-stage metrics*—such as the timing performance—that measure the final chip quality. This is mainly because of the high computational costs associated with performing post-placement stages for evaluating such metrics, making the *online* optimization impractical. Consequently, these optimizations struggle to align with actual performance improvements and can even lead to severe manufacturing issues. To bridge this gap, we propose **LaMPlace**, which **L**earns **a** **M**ask for optimizing cross-stage metrics in macro placement. Specifically, LaMPlace trains a predictor on *offline* data to estimate these *cross-stage metrics* and then leverages the predictor to quickly generate a mask, i.e., a pixel-level feature map that quantifies the impact of placing a macro in each chip grid location on the design metrics. This mask essentially acts as a fast evaluator, enabling placement decisions based on *cross-stage metrics* rather than *intermediate surrogate metrics*. Experiments on commonly used benchmarks demonstrate that LaMPlace significantly improves the chip quality across several key design metrics, achieving an average improvement of 9.6%, notably 43.0% and 30.4% in terms of WNS and TNS, respectively, which are two crucial cross-stage metrics that reflect the final chip quality in terms of the timing performance.

1 Introduction

Electronic Design Automation (EDA) aims to streamline the chip design process through efficient automation techniques (MacMillen et al., 2000; Markov et al., 2012). It involves a lengthy workflow that includes several stages such as logic synthesis, floorplanning, placement, clock tree synthesis (CTS), and routing, with the ultimate goal of optimizing the **p**erformance, **p**ower, and **a**rea (PPA) metrics of the final chip product (Rabaey et al., 2002; Wang et al., 2009). Within this workflow, macro placement is a crucial step, which involves positioning large rectangular circuit modules—such as memories, customized IPs, and interfaces—on a chip canvas. It determines the overall chip layout and impacts subsequent stages such as cell placement, CTS, and routing, thus significantly influencing the final PPA objectives (Chen et al., 2023).

Recent advances have shown that machine learning (ML) techniques have a promising potential in enhancing macro placement. These techniques are expected to autonomously explore the vast design space and generate chip layouts that are comparable to, or even superior to, those designed by human experts, while significantly reducing the time required for placement and shortening time-to-market. Traditionally, the macro placement task has been viewed as a black-box optimization (BBO) problem, tackled with optimization techniques such as simulated annealing (SA) and evolutionary algorithms (EA) (Kirkpatrick et al., 1983; Ho et al., 2004; Murata et al., 1995; Shi et al., 2023). In their work AlphaChip, published on *Nature*, Mirhoseini et al. (2021) first proposed to model macro placement as a Markov decision process (MDP), where the positions of macros are sequentially determined, and they addressed the problem using reinforcement learning (RL). Since then, there has been a surge of research on RL-based methods for macro placement (Cheng & Yan, 2021; Cheng et al., 2022; Lai et al., 2022; 2023; Geng et al., 2024).

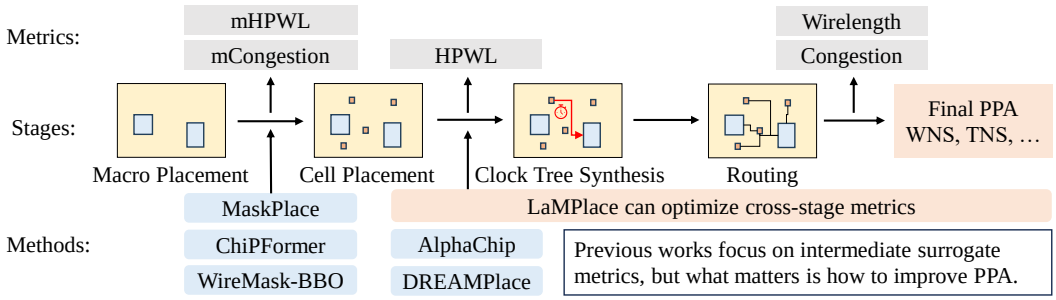

Figure 1: **Illustration of post-placement stages in the EDA workflow, the metrics available at each stage, and the optimization objectives of some previous works.** Our main contribution is to optimize the cross-stage metrics to improve the final PPA, rather than intermediate surrogate metrics.

Despite the achievements, existing methods primarily focus on optimizing intermediate surrogate metrics that are readily available at the current stage (see Figure 1). To name a few, MaskPlace (Lai et al., 2022), ChiPFormer (Lai et al., 2023), WireMask-BBO (Shi et al., 2023), and Efficient-Place (Geng et al., 2024) all focus on efficient optimization of the macro half-perimeter wire length (mHPWL), which is available immediately after macro placement, without considering standard cells (the relatively smaller components). AlphaChip (Mirhoseini et al., 2021) and DREAM-Place (Lin et al., 2019; 2020; Gu et al., 2020; Liao et al., 2022) mainly optimize the full-netlist half-perimeter wire length (HPWL) and congestion, which are available after cell placement but before CTS. Although DeepPR (Cheng & Yan, 2021) and PRNet (Cheng et al., 2022) propose to optimize the wirelength (WL) by integrating placement and routing, they do not consider the CTS stage and often produce infeasible outcomes due to overlaps. These intermediate surrogate metrics are commonly favored by RL and BBO methods because of their relatively low computational costs. However, as noted by a recent work (Wang et al., 2024), there exists a considerable misalignment between the surrogate metrics and the PPA metrics, such as worst negative slack (WNS) and total negative slack (TNS), which actually reflect the final chip quality but have not yet been adequately considered in the AI community (Cheng et al., 2023). Incorporating these design metrics at the macro placement stage is crucial for aligning with the industry's ongoing pursuit of the **"shift-left"** (Chen et al., 2024), i.e., advancing key processes earlier in the development cycle to improve outcome predictability and efficiency. The oversight on these essential metrics primarily arises from two reasons. On one hand, RL and BBO methods typically require extensive evaluations (i.e., reward computations) during online optimization. On the other hand, the PPA metrics are inherently cross-stage metrics, and evaluating them is highly time-consuming, requiring not only a full placement, including macro and cell placement, but also post-placement stages such as CTS and routing. The substantial time costs make the online optimization practice of RL and BBO impractical.

To tackle the aforementioned challenge, we propose **LaMPlace**, a novel method that **L**earns **a** **M**ask for optimizing cross-stage metrics in macro placement. LaMPlace offers two principle insights for macro placement. First, to mitigate the high computational costs of online optimization, we adopt a supervised learning paradigm, training a predictor for desired metrics on offline data. This offline setting is practical in industry, as substantial chip data can be collected from chip design projects. The trained predictor serves as a placement simulator, allowing for the estimation of cross-stage metrics at a relatively low computational cost. Second, to facilitate efficient placement, we shift from learning a predictor that outputs a single value for each placement to learning to generate a mask, i.e., a pixel-level feature map that quantifies the incremental objectives as each macro is placed sequentially. To achieve this, we model the predictor as a polynomial function of pair-wise distances between macros, with learnable coefficients. This polynomial formulation allows us to quickly generate a mask to guide the placement decisions in real-time. Leveraging this mask, LaMPlace employs a simple yet effective greedy policy, sequentially placing macros while maintaining local optimality at each step. We evaluate the effectiveness of our proposed LaMPlace on commonly used benchmarks, considering several cross-stage design metrics. The results demonstrate that LaMPlace significantly improves the chip quality across these metrics, achieving an average improvement of 9.6%, notably 43.0% and 30.4% in terms of WNS and TNS, respectively, which are two crucial cross-stage metrics that reflect the final chip quality in terms of the timing performance.

2 PRELIMINARIES

2.1 MACRO PLACEMENT

Chip placement involves strategically arranging a set of chip modules, including macros (large modules such as memories, customized IPs, and interfaces) and cells (small modules like logic gates), on a chip canvas, subject to the non-overlap constraint. As an integral part of the entire EDA workflow, the ultimate goal of macro placement—and indeed, all these related steps—is to optimize the **p**ower, **p**erformance, and **a**rea (PPA) metrics of the final chip product. As illustrated in Figure 1, evaluating the final PPA involves several stages and is very time-consuming. Therefore, a variety of heuristic metrics have been proposed in order to guide the optimization at intermediate stages. In this section, we present some important concepts and metrics to facilitate a better understanding of the macro placement task (Rabaey et al., 2002; Wang et al., 2009).

PPA refers to performance, power, and area, which are three key dimensions to assess the quality of a chip product. These are not measured by a single metric but through a series of critical metrics. They include, but are not limited to, worst negative slack (WNS), total negative slack (TNS), number of violating paths (NVP), and physical area utilization. Optimizing the PPA metrics, as a fundamental objective of EDA, has been extensively explored in the industry through expert-designed heuristics. However, in the AI community, the challenge of PPA optimization has not been adequately recognized (Wang et al., 2024). Bridging this gap and enhancing the integration of AI strategies in PPA optimization are core aspirations of this paper.

Worst Negative Slack (WNS) and Total Negative Slack (TNS) are crucial metrics to assess the timing performance of a chip circuit. Slack refers to the difference between a signal's expected and required arrival times, and negative slack indicates a timing violation. WNS identifies the worst negative slack in a circuit, highlighting the most critical timing issue, while TNS sums up all negative slacks, reflecting the overall timing issues. These two metrics, as representatives of PPA metrics, are considered as evaluation metrics to demonstrate the effectiveness of our method.

Congestion evaluates the density of wires in different chip regions. High congestion in certain areas can pose substantial challenges during the routing stage. While not a direct component of the PPA metrics, managing congestion effectively is essential to ensure that the chip can be successfully manufactured. Congestion is typically estimated after CTS but before detailed routing, allowing for adjusting macro placement and routing strategies to mitigate potential issues. It is also used as an evaluation metric in this paper.

Wire Length (WL) is the total length of all wires connecting all modules in a chip. **half-perimeter Wire Length (HPWL)** is the sum of half-perimeters of bounding boxes that encompass all pins in each net. It is widely used as an estimation of WL and is obtained after cell placement. **Macro HPWL (mHPWL)** further simplifies HPWL by only considering the macros. It is favored in recent studies as it can be immediately obtained after macro placement. These metrics are thought to correlate with the final PPA, but they do not directly reflect the chip quality. In this paper, we include HPWL as an evaluation metric mainly for a better comparison with previous methods, demonstrating the effectiveness of our approach for optimizing cross-stage metrics.

2.2 RELATED WORK

Existing methods for macro placement can be roughly categorized into analytical methods, black-box optimization (BBO)-based methods, and reinforcement learning (RL)-based methods.

Analytical methods formulate the optimization objective, such as HPWL, as an analytical function of module coordinates, which is solvable via quadratic programming (Kahng et al., 2005; Viswanathan et al., 2007a;b; Spindler et al., 2008; Chen et al., 2008; Kim et al., 2012; Kim & Markov, 2012; Cheng et al., 2018) or direct gradient descent (Lin et al., 2019; 2020; Gu et al., 2020; Liao et al., 2022). Although efficient, they rely on differentiable surrogate metrics and struggle with complex and black-box PPA metrics.

BBO-based methods view macro placement as a BBO problem and solve it using algorithms like SA and EA (Kirkpatrick et al., 1983; Ho et al., 2004; Murata et al., 1995; Shi et al., 2023; Sherwani, 2012; Shunmugathammal et al., 2020; Vashisht et al., 2020; Murata et al., 1996; Chang et al.,

2000; Roy et al., 2006; Khatkhate et al., 2004). They require numerous evaluations, which are highly time-consuming when considering cross-stage metrics. Notably, WireMask-BBO (Shi et al., 2023) introduces an efficient greedy algorithm for optimizing mHPWL based on the concept of wiremask (Lai et al., 2022). In this work, we develop a learnable mask instead of the wiremask, and adopt the greedy algorithm from Shi et al. (2023) for efficient optimization.

RL-based methods have recently emerged, starting from AlphaChip (Mirhoseini et al., 2021), which first modeled macro placement as a Markov Decision Process (MDP). DeepPR (Cheng & Yan, 2021) and PRNet (Cheng et al., 2022) integrate placement and routing but do not consider CTS and the non-overlap constraint. MaskPlace (Lai et al., 2022) introduces the wiremask concept, later adopted by Shi et al. (2023) and Geng et al. (2024) to significantly improve efficiency. The successful application of wiremask also motivates us to learn a mask for fast macro placement. These methods require extensive online learning steps, making it challenging to directly optimize PPA as rewards. ChiPFormer (Lai et al., 2023) employs offline RL to reduce the online learning costs. However, it relies on a pre-trained expert policy and does not adequately consider the desired metrics. Additionally, achieving an optimal performance still requires extensive online fine-tuning steps.

2.3 WIREMASK FOR FAST MHPWL OPTIMIZATION

The concept of wiremask was first introduced by Lai et al. (2022) and later adopted by Shi et al. (2023) and Geng et al. (2024) for fast optimization of the macro half-perimeter wire length (mHPWL). Figure 2 illustrates the wiremask with a trivial example. In the left figure, M_1 and M_2 represent two macros that have already been placed, and M_3 represents the next macro to be placed. The red and green solid boxes indicate the bounding boxes of two nets. The current mHPWL is the sum of half-perimeters of these boxes, i.e., mHPWL $= w_1 + h_1 + w_2 + h_2$. When M_3 is placed at a specific grid position, we can easily calculate the increment of mHPWL. Here we use the bottom-left corner of macros to denote their positions. As shown in the right figure, the wiremask is a matrix that quantifies the increase in mHPWL resulting from placing M_3 at each specific grid position. The wiremask can be computed quickly because the mHPWL increment is an explicit function of the macro positions. To determine the next macro position, we can first calculate the wiremask and then greedily select a feasible position that results in the smallest mHPWL increase. Empirical results from Shi et al. (2023) and Geng et al. (2024) demonstrate that this greedy approach yields sufficiently good mHPWL performance.

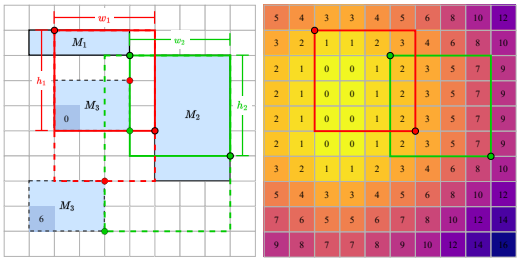

Figure 2: An example from Geng et al. (2024) to illustrate of the concept of the wiremask.

Motivation of LaMPlace If we learn a predictor with the full placement as input, it can serve as a sparse reward model. However, its black-box nature makes it hard to develop an optimization algorithm as efficient as the one with wiremask. This insight motivates us to explore **how to learn a mask for more general metrics**, similar to how wiremask works for mHPWL. We recognize that mHPWL is essentially in form of a combination of (Manhattan) distances between macros, enabling fast calculation of the mHPWL increase at each position and each step. We further observe that the computational principles behind wiremask can be generalized to any polynomial functions with respect to pair-wise distances between macros. This motivates us to **learn a predictor in form of polynomials and leverage it to generate a mask** to guide the optimization process.

3 METHODOLOGY

This section introduces our proposed framework LaMPlace. An overview of LaMPlace is shown in Figure 3, which outlines two main components. First, we train a predictor for the cross-stage metrics using Laurent polynomial approximation. The coefficients of the polynomials are treated as learnable flows, which we refer to as **L-flows**. Second, we leverage the trained predictor to generate a mask, termed as **L-mask**, to guide the efficient macro placement. We present detailed explanations

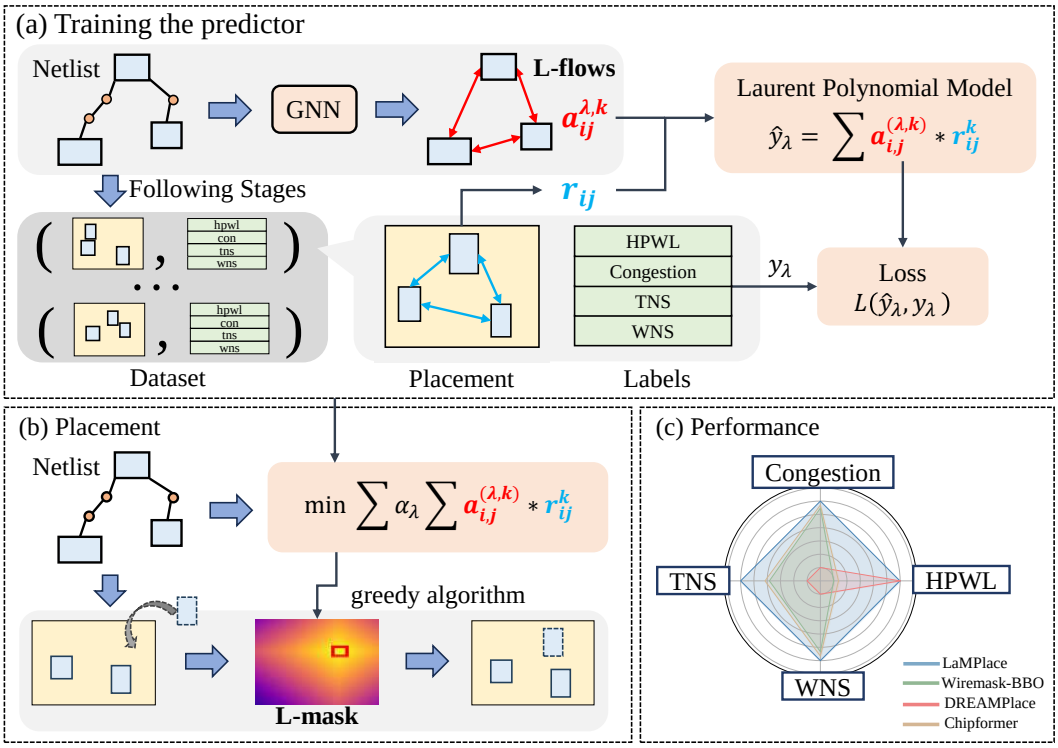

Figure 3: **Overview of LaMPlace.** (a) We construct an offline dataset by executing placement and post-placement stages to obtain placement solutions and their corresponding cross-stage metrics. A predictor in form of a Laurent polynomial is trained on this dataset. (b) Using the trained predictor, we reformulate the macro placement task as a polynomial optimization problem. We leverage the predictor to generate the L-mask to guide the sequentially greedy algorithm for fast placement. (c) LaMPlace outperforms existing methods across several key design metrics. The results are averaged over 8 chip circuits and then normalized to $[0, 1]$ for a better visualization.

of these components in Section 3.1 and Section 3.2, respectively. Additional implementation details can be found in Appendix A. We will release the code once the paper is accepted.

3.1 Predicting Metrics Using Laurent Polynomial Approximation

Graph Representation A chip netlist consists of various nets representing the interconnections between macros and standard cells. We represent a netlist as a graph $G(V, E)$, where V denotes the nodes and E the edges. Given the high number of standard cells—often surpassing $100,000$ in a single chip—it is impractical or inefficient to represent all macros and cells as individual nodes. Therefore, consistent with previous works, in our graph representation, each node represents a macro. However, unlike prior approaches that disregard standard cells in the graph representation, we incorporate standard cell information by introducing edge features that quantify the connectivity between macros, taking into account paths that include standard cells. Specifically, these edge features capture the number of pathways connecting two macros, with paths differentiated by the number of standard cells they traverse. Such a representation enables us to take the standard cells into consideration with a relatively low computational overhead. More details about the node and edge features can be found in Appendix A.1.

Laurent Polynomial Approximation Based on the aforementioned graph representation, we adopt a graph neural network (GNN), denoted as $\mathrm{GNN}_{\boldsymbol{\theta}}$, to extract node features $\boldsymbol{h}_v$ for each node $v \in V$. These features are stacked as a matrix $\boldsymbol{H} = (\boldsymbol{h}_1, \cdots, \boldsymbol{h}_{|V|})^\top \in \mathbb{R}^{|V| \times d}$, writing $\boldsymbol{H} = \mathrm{GNN}_{\boldsymbol{\theta}}(G)$. We consider a set of Λ metrics, which are evaluated using EDA tools. In this work, we consider 4 different cross-stage metrics, including HPWL, congestion, WNS, and

TNS. Each evaluation metric y_λ is supposed as a function of the netlist G and the macro positions $\boldsymbol{X} = (\boldsymbol{x}_1, \cdots, \boldsymbol{x}_{|V|})^\top \in \mathbb{R}^{|V|\times 2}$, writing $y_\lambda = f_\lambda(\boldsymbol{H}, \boldsymbol{X})$, where $f_\lambda(\cdot)$ represents a EDA tool to run the post-placement stages and obtain the final metrics. Notably, this function is translation-invariant[1] with respect to the macro positions. Therefore, we re-express it as a function of the pairwise distances $r_{i,j}(\boldsymbol{X}) = \|\boldsymbol{x}_i - \boldsymbol{x}_j\|_2$ between every two macros i and j.

We predict each metric y_λ using a Laurent polynomial function of the pair-wise distances:

$$\hat{y}_\lambda = \hat{f}_\lambda(\boldsymbol{H}, \boldsymbol{X}) = \sum_{k\in K} \sum_{1\le i<j\le |V|} a_{i,j}^{(\lambda,k)}(\boldsymbol{H}) \cdot \|\boldsymbol{x}_i - \boldsymbol{x}_j\|_2^k. \tag{1}$$

In Formula 1, K denotes a set of integers indicating the exponents in the polynomial, and $a_{i,j}^{(\lambda,k)}(\boldsymbol{H})$ are the coefficients, calculated as:

$$a_{i,j}^{(\lambda,k)}(\boldsymbol{H}) = \frac{1}{2}\left(\boldsymbol{h}_i^\top \boldsymbol{M}^{(\lambda,k)} \boldsymbol{h}_j + \boldsymbol{h}_j^\top \boldsymbol{M}^{(\lambda,k)} \boldsymbol{h}_i\right), \tag{2}$$

where $\boldsymbol{M}^{(\lambda,k)} \in \mathbb{R}^{d\times d}$ are learnable weight matrices. Intuitively, each $a_{i,j}^{(\lambda,k)}$ captures the relationship between two macros i and j, analogous to the concept of flows in networks. Therefore, we refer to these coefficients as **"learnable flows"**, or **"L-flows"**. Further discussions are in Appendix A.2.

Training the Predictor To train the predictor, we construct a dataset $\mathcal{D}$ using a collection of C chip netlists $\{G_c\}_{c=1}^C$, each represented as a graph G_c. For each netlist, we generate a set of M different placements $\{\boldsymbol{X}_{c,m}\}_{m=1}^M$ by running the available placement tool like DREAMPlace with different seeds. Subsequent stages—such as cell placement, clock tree synthesis (CTS), and routing—are run with existing EDA tools to yield the cross-stage evaluation metrics $y_{c,m}^{(\lambda)} = f_\lambda(G_c, \boldsymbol{X}_{c,m})$ for each $\lambda \in [\Lambda]$. Then we obtain a dataset

$$\mathcal{D} = \left\{ \left(G_c, \boldsymbol{X}_{c,m}, y_{c,m}^{(\lambda)}\right) \middle| c \in [C], m \in [M], \lambda \in [\Lambda] \right\}. \tag{3}$$

For each chip G_c and placement $\boldsymbol{X}_{c,m}$, we give the predict as $\hat{y}_{c,m}^{(\lambda)} = \hat{f}_\lambda(\mathrm{GNN}_{\boldsymbol{\theta}}(G_c), \boldsymbol{X}_{c,m})$. We use the MSE loss to train the predictor:

$$L_{\text{MSE}} = \frac{1}{CM\Lambda} \sum_{c,m,\lambda} \left(\hat{y}_{c,m}^{(\lambda)} - y_{c,m}^{(\lambda)}\right)^2. \tag{4}$$

We additionally adopt a pair-wise ranking loss to boost the training effectiveness, which is defined as:

$$L_{\text{Rank}} = \sum_\lambda \sum_{y_{c_1,m_1}^{(\lambda)} > y_{c_2,m_2}^{(\lambda)}} Z_{c_1,m_1,c_2,m_2} \log\left(1 + \exp\left(\hat{y}_{c_2,m_2}^{(\lambda)} - \hat{y}_{c_1,m_1}^{(\lambda)}\right)\right), \tag{5}$$

where

$$Z_{c_1,m_1,c_2,m_2} = \left| \frac{\exp\left(y_{c_1,m_1}^{(\lambda)}\right) - \exp\left(y_{c_2,m_2}^{(\lambda)}\right)}{\sum_{c,m} \exp\left(y_{c,m}^{(\lambda)}\right)} \right| \tag{6}$$

are weighted coefficients defined following previous works (Chen et al., 2023). We use the combination of these two loss functions to effectively train the predictor:

$$L = \beta_1 \cdot L_{\text{MSE}} + \beta_2 \cdot L_{\text{Rank}}, \tag{7}$$

where β_1, β_2 are hyperparameters.

3.2 Learnable-Mask-Guided Greedy Algorithm For Efficient Placement

Optimization Problem Formulation In the macro placement phase, the chip canvas is discretized as an $N \times N$ grid, and the feasible macro positions are the grid corners, denoted as $\mathcal{X}$. With the predictor in hand, the task of macro placement is recast as an optimization problem. Without loss of

[1] Here 'translation-invariant' is an approximate description, indicating that the target metrics are primarily influenced by the relative positions of macros.

generality, we assume that, for all metrics, a lower value indicates better performance. Formally, the goal is to minimize the predicted metrics subject to no overlap:

$$\begin{aligned} \underset{\boldsymbol{X}\in\mathcal{X}^{|V|}}{\arg\min} \quad & \sum_{\lambda\in[\Lambda]} \alpha_\lambda \hat{f}_\lambda(\boldsymbol{H},\boldsymbol{X}) \\ \text{s.t.} \quad & \text{Overlap}(G,\boldsymbol{X}) = 0, \end{aligned} \tag{8}$$

where $\hat{f}_\lambda(\boldsymbol{H},\boldsymbol{X})$ are polynomial functions defined in Equation 1, and α_λ are hyperparameters. Unlike wiremask, an advantage of our method is the ability to control the weights of every metrics, effectively balancing the multi-objective optimization problem.

Efficient Greedy Policy Despite the simple polynomial formulation, solving the above optimization problem is still challenging due to the large number of macros and the non-overlap constraint. This highlights the necessity of the polynomial form of the predictor, which enables us to design a greedy algorithm for fast placement. Specifically, we sequentially determine the position of one macro at each step. At the tth step, the positions of the first $t-1$ macros are already determined. We place the tth macro position greedily by solving the following problem:

$$\begin{aligned} \underset{\boldsymbol{x}_t\in\mathcal{X}}{\arg\min} \quad & \Delta_t(\boldsymbol{x}_t) = \sum_{\lambda\in[\Lambda]} \alpha_\lambda \sum_{k\in K} \sum_{i=1}^{t-1} a_{i,t}^{(\lambda,k)}(\boldsymbol{H}) \cdot \|\boldsymbol{x}_t - \boldsymbol{x}_i\|_2^k \\ \text{s.t.} \quad & \text{Overlap}(G,\boldsymbol{x}_1,\cdots,\boldsymbol{x}_t) = 0. \end{aligned} \tag{9}$$

Generating Learnable Mask In Formula 9, $\Delta_t(\boldsymbol{x}_t)$ represents the increase of the objective function from Formula 8 when placing the new macro at the grid $\boldsymbol{x}_t$. The matrix Δ_t containing $\Delta_t(\boldsymbol{x}_t)$ values for all $\boldsymbol{x}_t \in \mathcal{X}$ is analogous to the wiremask used in the previous works (Lai et al., 2022; Shi et al., 2023; Geng et al., 2024), which has shown promising potential in improving placement efficiency (Shi et al., 2023). As our $\Delta_t(\boldsymbol{x}_t)$ is learnable rather than pre-defined by mHPWL, it extends wiremask to any learnable metrics. Therefore, we refer to Δ_t as a **"learnable mask"**, or an **"L-Mask"**. Thanks to the polynomial form of the predictor, the L-mask can be computed very efficiently. Notice that the coefficients $a_{i,j}^{(\lambda,k)}$ are position-agnostic and need to be computed only once before the placement process:

$$\boldsymbol{A}^{(\lambda,k)} = \frac{1}{2}\boldsymbol{H}\left(\boldsymbol{M}^{(\lambda,k)} + \boldsymbol{M}^{(\lambda,k)\top}\right)\boldsymbol{H}^\top, \quad a_{i,j}^{(\lambda,k)} = \left[\boldsymbol{A}^{(\lambda,k)}\right]_{i,j}. \tag{10}$$

Here $\boldsymbol{A}^{(\lambda,k)}$ is the matrix with $a_{i,j}^{(\lambda,k)}$ as entries, indicating the L-flow between each pair of macros. This approach keeps the computational cost of the GNN module very low. At each step t during placement, we only need to calculate the distances between each grid position and the placed macros, which can be efficiently computed through tensor computation. See Algorithm 1 for more details.

L-Mask-Guided Black-Box Optimization The L-mask derives an efficient greedy placement policy, which can be used to boost any sequential placement approach by restricting the solution space. In this paper, we showcase its application within the WireMask-BBO framework proposed by Shi et al. (2023). Specifically, in this framework, the placement task is recast as a BBO problem, with the macro positions as the optimization variables. The genotype solutions are randomly initialized and optimized using the algorithms such as EA. For each genotype solution, we use the L-mask to record the increment of target metrics and greedily improve the genotype solution by sequentially moving the macros to the nearest optimal grid. See Algorithm 2 for more details.

4 EXPERIMENTS

4.1 EXPERIMENTAL SETUP

Benchmarks We primarily assess our method on the ICCAD2015 benchmark (Kim et al., 2015), which consists of eight large-scale chip circuits. Notably, some recent works (Cheng & Yan, 2021; Cheng et al., 2022; Lai et al., 2022; 2023; Shi et al., 2023) have commonly used benchmarks from ISPD2005 (Nam et al., 2005) and ICCAD2004 (Adya et al., 2009). However, the circuits in these

benchmarks are in a simplified `Bookshelf` format, lacking the original `LEF/DEF` files and missing design information necessary for evaluating PPA in later stages. Consequently, obtaining PPA metrics on these benchmarks is infeasible. In contrast, the circuits in the ICCAD2015 benchmarks are from the ICCAD2015 contest for timing-driven placement. They include timing libraries and design constraints, allowing for proper evaluation. More details can be found in Appendix A.4. Additionally, we assess the zero-shot generalization capability of LaMPlace on a recently released benchmark, ChipBench (Wang et al., 2024). ChiPBench provides an opensource dataset, containing 6 industry circuits, and a comprehensive benchmark for PPA evaluation.

Baselines We compare LaMPlace with several recent advanced placement methods. DREAMPlace (Lin et al., 2019; 2020; Gu et al., 2020; Liao et al., 2022) is an analytical method initially designed for cell placement. We use its latest version, which integrates timing optimization, to perform mixed-size placement, moving both macros and standard cells together. WireMask-BBO (Shi et al., 2023) is a recent state-of-the-art method for optimizing mHPWL. It implements various BBO algorithms, with WireMask-EA demonstrating the best overall performance, so we use WireMask-EA for comparison. The placement algorithm of LaMPlace operates under the same settings as WireMask-EA but utilizes our learned L-mask instead of the wiremask. ChiPFormer (Lai et al., 2023) is a representative RL-based method, which has been pre-trained on an offline dataset. We load their pre-trained model and fine-tune it on each circuit for comparison.

Evaluations Metrics As explained in Section 2.1, we use four key metrics for evaluation: HPWL, congestion (Cong.), WNS, and TNS. These metrics are crucial for improving the final chip quality but are time-consuming to evaluate as they involve stages after macro placement. For better reproducibility, we use open-source tools to estimate the desired metrics. Specifically, we run DREAMPlace (Liao et al., 2022) for cell placement to report HPWL and congestion, and OpenTimer (Huang & Wong, 2015) for timing analysis to estimate WNS and TNS. Although the model is not directly trained on the final PPA metrics obtained after all stages, our experiments have demonstrated its effectiveness in optimizing cross-stage metrics and ultimately improving the final PPA.

Training and Inference For training LaMPlace, we use the first six circuits in ICCAD2015 for training, specifically *superblue1, 3, 4, 5, 7,* and *10*. The last two circuits, *superblue16* and *18*, are excluded from the training set to demonstrate generalization to unseen data. This is a default dataset partition just according to the circuit indices. We run DREAMPlace for mixed-size placement to generate 200 layouts for each training circuit and evaluate them to obtain the desired metrics, which serve as training labels. This process results in a dataset of $1,200$ placement-labels pairs as the offline dataset. Notably, this requires only $1,200$ evaluations in total on all six training circuits, significantly fewer than RL and BBO methods, which typically require tens of thousands of steps for convergence on each circuit. The predictor is trained on this dataset and then tested on all circuits.

As LaMPlace, WireMask-EA, and ChiPFormer share the same Python implementation for the canvas, we implement them under the same settings, where the chip canvas is divided into an 84×84 grid. For LaMPlace and Wiremask-EA, we execute the EA algorithm with 50 initial random rounds followed by 20 evolutionary rounds. For ChiPFormer, we load their pre-trained model and fine-tune it for $2,000$ steps. For DREAMPlace, we run it for mixed-size placement using its default parameters, with the timing optimization process enabled. More details can be found in Appendix A.5.

4.2 Main Results

Table 1 presents the main evaluation results for macro placement using different approaches. The results show that LaMPlace outperforms other baselines. Specifically, LaMPlace consistently achieves the best average rank and the best timing results (i.e., the best TNS and WNS) across all cases, and achieves the best congestion on almost all cases. For HPWL, it achieves comparable performance with DREAMPlace, which directly optimizes HPWL as an analytical objective, and significantly surpasses other methods. LaMPlace achieves an average improvement of 9.6% across the four metrics, compared to the best-performing performing methods on each of these metrics. Notably, it achieves improvements of 43.0% and 30.4% on TNS and WNS, respectively. The overall performance is visualized as a radar chart in Fig 3 (c). We visualize the obtained placement solutions in Appendix B.8. We report the running time in Appendix B.6. We further conduct experiments on ChiPBench Wang et al. (2024), which evaluates the post-routing PPA results. We run the placement algorithm of LaMPlace directly on the industrial chips from ChiPBench without any fine-tuning. The results are in Table 4 in Appendix B.1, which demonstrate that LaMPlace still outperform other baselines on ChiPBench, demonstrating LaMPlace's zero-shot generalization ability.

Table 1: **Comparisons of HPWL** ($\times 3.8 \times 10^{11}$ um)**, Cong.** ($\times 10^{-2}$)**, TNS** ($\times 10^{5}$ps)**, and WNS** ($\times 10^{3}$ps) **for macro placement derived by different approaches.** For HPWL and Cong., lower is better, while for TNS and WNS, higher is better. The results for DREAMPlace, Wiremask-EA and LaMPlace are obtained from three independent runs with different random seeds, and we report the mean and standard deviations (mean±std) of each metric. Additionally, we report the average rank of these methods on each circuit. We mark the best results in **bold red**, and we mark the second best results in underlined blue.

		superblue1	superblue3	superblue4	superblue5	superblue7	superblue10	superblue16	superblue18
DREAMPlace	HPWL	**25.72 (±3.70)**	**7.42 (±0.76)**	11.12 (±2.38)	**6.12 (±1.44)**	3.26 (±0.18)	**17.35 (±2.24)**	**2.30 (±0.05)**	36.07 (±8.93)
	Cong.	2.02 (±0.06)	2.92 (±0.01)	1.62 (±0.02)	1.92 (±0.19)	1.13 (±0.09)	1.41 (±0.03)	2.20 (±0.01)	1.03 (±0.11)
	TNS	-5210.15 (±108.89)	-8029.97 (±2480.47)	-3764.22 (±417.03)	-22321.9 (±6238.18)	-7374.28 (±2188.93)	-7812.76 (±189.47)	-1526.1 (±33.52)	-751.27 (±249.91)
	WNS	-144.74 (±18.58)	-1335.9 (±346.77)	-241.24 (±66.36)	-3928.92 (±2760.68)	-414.00 (±199.55)	-339.27 (±118.58)	-107.05 (±1.16)	-88.11 (±10.53)
	Rank	2.75	3.25	3.50	3.25	3.00	2.75	2.25	3.50
WireMask-EA	HPWL	85.71 (±17.34)	17.68 (±1.32)	8.17 (±3.75)	34.94 (±7.47)	5.39 (±1.06)	21.27 (±0.88)	11.74 (±1.98)	38289.15 (±6660.46)
	Cong.	1.87 (±0.10)	2.48 (±0.02)	1.79 (±0.39)	1.84 (±0.04)	1.46 (±0.08)	1.19 (±0.02)	1.56 (±0.41)	1.00 (±0.04)
	TNS	-2524.56 (±164.00)	-2132.54 (±154.44)	-1966.08 (±208.84)	**-2553.51 (±414.32)**	-1628.77 (±109.99)	-8370.46 (±1070.55)	-18343.30 (±16445.55)	**-406.01 (±100.69)**
	WNS	-155.00 (±23.15)	-293.85 (±34.09)	-107.72 (±21.13)	-194 (±25.71)	-76.86 (±3.88)	-290.46 (±60.06)	-635.89 (±601.41)	-78.25 (±8.65)
	Rank	3.25	2.25	2.75	2.50	3.00	2.75	3.25	2.50
ChiPFormer	HPWL	68.10	33.37	8.36	31.06	7.40	24.47	16.58	3528.80
	Cong.	2.05	2.49	1.92	**0.95**	1.87	1.19	**1.28**	1.00
	TNS	**-2150.53**	-2447.33	-1586.05	-3176.20	**-1489.84**	-7862.58	-15426.07	-378.90
	WNS	-132.74	-229.20	-85.28	-202.47	-68.99	-256.34	-322.05	-80.57
	Rank	2.50	3.00	2.75	2.50	3.00	2.75	2.75	2.75
LaMPlace	HPWL	49.17 (±15.71)	22.25 (±2.91)	**4.47 (±1.94)**	31.48 (±6.25)	**3.22 (±0.29)**	22.13 (±2.66)	7.61 (±0.51)	**16.94 (±7.14)**
	Cong.	**1.51 (±0.04)**	**2.34 (±0.03)**	**1.54 (±0.07)**	1.54 (±0.15)	**0.87 ±0.04**	**1.06 (±0.02)**	2.03 (±0.01)	**0.74 (±0.02)**
	TNS	-2422.01 (±272.73)	**–1797.7 (±115.81)**	**-1424.31 (±63.10)**	-2889.21 (±121.14)	-1585.32 (±201.6)	**-7613.01 (±453.81)**	**-1514.73 (±524.61)**	-426.91 (±52.83)
	WNS	**-127.31 (±13.23)**	**-174.94 (±46.02)**	**-84.01 (±9.61)**	**-178.18 (±29.39)**	**-66.02 (±7.28)**	**-224.34 (±21.05)**	**-36.87 (±11.04)**	**-66.93 (±11.62)**
	Rank	**1.50**	**1.50**	**1.00**	**1.75**	**1.25**	**1.50**	**1.75**	**1.25**

4.3 ANALYSIS

Case Study We visualize the placement results for the compared methods in Figure 4. In this case, existing methods exhibit excellent mHPWL results, but LaMPlace outperforms them on the actual design metrics. Notably, LaMPlace tends to place macros along the borders of the canvas, reserving the center for standard cells. This is a behavior of experienced designers, because this strategy, though increasing mHPWL, can improve the final results empirically (Chiou et al., 2016). Surprisingly, LaMPlace discovers this optimization technique without any prior knowledge. We further use a commercial EDA tool, Cadence *Innovus*, to analyze the final PPA results, demonstrating the effectiveness of LaMPlace to actually enhance the chip quality. The results are in Apendix B.2.

Correlation Analysis To underscore the significance of cross-stage metric optimization, validate our motivation, and provide insights to the research community, we present the correlations between the metrics involved in this work in Figure 5. The results are derived by collecting all layouts generated by the tested methods on all circuits. We calculate pair-wise Pearson correlation coefficients, which reflect their linear correlations. Figure 5(a) illustrates the correlation coefficients between the four evaluation metrics. The results indicate that HPWL and congestion exhibit a positive correlation, and TNS and WNS also show a positive correlation. However, HPWL and congestion do not significantly correlate with TNS and WNS. This suggests that placement is a complex multi-objective optimization problem, and optimizing a single metric alone is insufficient. Figure 5(b) shows the correlation between the evaluation metrics and different optimization surrogates. The results show that the predicted values strongly positively correlate with the true metrics. In contrast, the commonly used intermediate surrogate metric, mHPWL, fails to positively correlate with all the

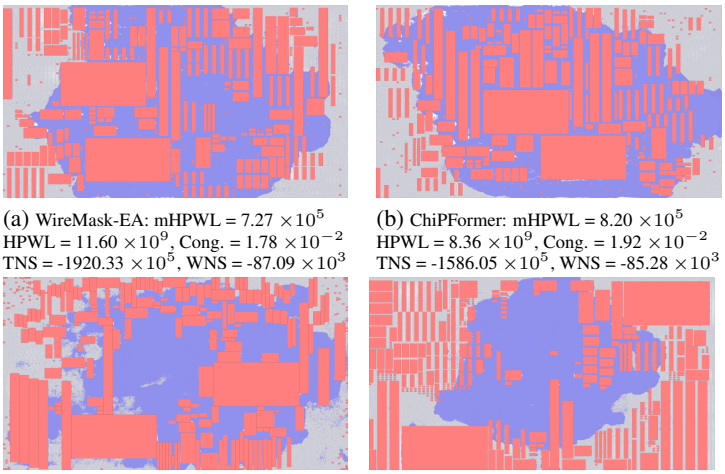

(a) WireMask-EA: mHPWL = 7.27 $\times 10^5$
HPWL = 11.60 $\times 10^9$, Cong. = 1.78 $\times 10^{-2}$
TNS = -1920.33 $\times 10^5$, WNS = -87.09 $\times 10^3$

(b) ChiPFormer: mHPWL = 8.20 $\times 10^5$
HPWL = 8.36 $\times 10^9$, Cong. = 1.92 $\times 10^{-2}$
TNS = -1586.05 $\times 10^5$, WNS = -85.28 $\times 10^3$

(c) DREAMPlace: mHPWL = 22.80 $\times 10^5$
HPWL = 6.59 $\times 10^9$, Cong. = 1.39 $\times 10^{-2}$
TNS = -1871.03$\times 10^5$, WNS = -107.80 $\times 10^3$

(d) LaMPlace : mHPWL = 100.66 $\times 10^5$
HPWL = 2.48 $\times 10^9$, Cong. = 1.04 $\times 10^{-2}$
TNS = -1451.41 $\times 10^5$, WNS = -77.61 $\times 10^3$

Figure 4: **Visualization of full-netlist placement results of *superblue4* using different methods.** Macros are marked in red, while standard cells are represented in blue. The evaluation metrics are labeled under each figure.

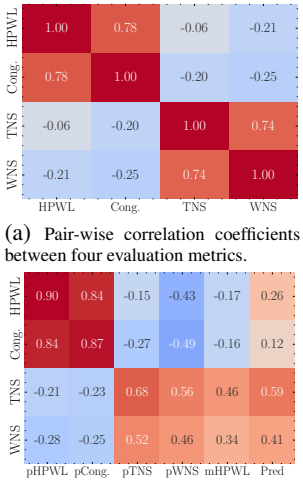

(a) Pair-wise correlation coefficients between four evaluation metrics.

(b) Correlation coefficients between mHPWL, predicted value of LaMPlace and four evaluation metrics.

Figure 5: **Correlation analysis.** The prefix 'p' denotes the predicted values and the 'Pred' represents the weighted sum of them.

metrics as our predictor does. The metric "Pred" represents the sum of predicted values, serving as the optimization objective for placement as introduced in Section 3.2. The results demonstrate that "Pred" has a positive correlation with all metrics, highlighting its effectiveness to serve as an optimization objective. These findings reveal the fundamental reasons for LaMPlace's superiority in multi-objective optimization compared to previous works.

Ablation Study We conduct comparative experiments to demonstrate the effectiveness of the Laurent polynomial form. Specifically, in Equation 1, we define K as a set of integers indicating the orders of terms in the polynomial. In the main experiments, we empirically set $K = \{1, 0, -1, -2\}$. We further investigate the effect of the choice of K, and the results are presented in Table 8 in Appendix B.3. The findings indicate that the Laurent polynomial form, rather than general polynomials, can indeed enhance performance.

As shown in Equation 8, the optimization objective during the placement phase is defined as $\hat{f} = \sum_{\lambda \in [\Lambda]} \alpha_\lambda \hat{f}_\lambda(\boldsymbol{H}, \boldsymbol{X})$, which is the weighted summation of different metrics, achieving a trade-off among these metrics. We further conduct experiments to investigate the impact of the hyper-parameters α_λ. Results are in Table 9 in Appendix B.4, which demonstrate that adjusting these hyperparameters can strategically control the weights of the metrics.

We also conduct an ablation study on the number of layers in the GNN architecture. The results are shown in Figure 12 in Appendix B.5, demonstrating that the model performance is overall robust against the GNN architecture.

Prediction Error Analysis We analyze the correlation between the placement quality and the prediction error. The results are shown in Figure 13 in Appendix B.7. The results demonstrate the positive correlation between the placement quality and the prediction error, while the placement quality is overall robust against the variations. We also present the training curves of several key metrics regarding the prediction error in Figure 14 in Appendix B.7.

5 Conclusions

In this paper, we propose LaMPlace, a novel macro placement method that learns a mask to optimizes cross-stage metrics, rather than intermediate surrogate metrics. It introduces a predictor, in form of Laurent polynomial functions, for cross-stage metrics. This formulation derives a sequentially greedy policy for efficient placement. Experiments demonstrate that LaMPlace can significantly improve the chip quality in terms of several key design metrics.

REPRODUCIBILITY STATEMENT

We provide the following information for the reproducibility of our proposed LaMPlace. The method is detailed in Section 3. The implementation details are provided in Appendix A. The experimental details and results are in Section 4 and further elaborated in Appendix A.5. Moreover, we will make our source code publicly available once the paper is accepted for publication.

REFERENCES

SN Adya, S Chaturvedi, and IL Markov. Iccad'04 mixed-size placement benchmarks. *GSRC Bookshelf*, 2009.

Yun-Chih Chang, Yao-Wen Chang, Guang-Ming Wu, and Shu-Wei Wu. B*-trees: A new representation for non-slicing floorplans. In *Proceedings of the 37th Annual Design Automation Conference*, pp. 458–463, 2000.

Lei Chen, Yiqi Chen, Zhufei Chu, Wenji Fang, Tsung-Yi Ho, Yu Huang, Sadaf Khan, Min Li, Xingquan Li, Yun Liang, et al. The dawn of ai-native eda: Promises and challenges of large circuit models. *arXiv preprint arXiv:2403.07257*, 2024.

Tung-Chieh Chen, Zhe-Wei Jiang, Tien-Chang Hsu, Hsin-Chen Chen, and Yao-Wen Chang. Ntuplace3: An analytical placer for large-scale mixed-size designs with preplaced blocks and density constraints. *IEEE Transactions on Computer-Aided Design of Integrated Circuits and Systems*, 27(7):1228–1240, 2008.

Yifan Chen, Jing Mai, Xiaohan Gao, Muhan Zhang, and Yibo Lin. Macrorank: Ranking macro placement solutions leveraging translation equivariancy. In *Proceedings of the 28th Asia and South Pacific Design Automation Conference*, pp. 258–263, 2023.

Chung-Kuan Cheng, Andrew B Kahng, Ilgweon Kang, and Lutong Wang. Replace: Advancing solution quality and routability validation in global placement. *IEEE Transactions on Computer-Aided Design of Integrated Circuits and Systems*, 38(9):1717–1730, 2018.

Chung-Kuan Cheng, Andrew B Kahng, Sayak Kundu, Yucheng Wang, and Zhiang Wang. Assessment of reinforcement learning for macro placement. In *Proceedings of the 2023 International Symposium on Physical Design*, pp. 158–166, 2023.

Ruoyu Cheng and Junchi Yan. On joint learning for solving placement and routing in chip design. *Advances in Neural Information Processing Systems*, 34:16508–16519, 2021.

Ruoyu Cheng, Xianglong Lyu, Yang Li, Junjie Ye, Jianye Hao, and Junchi Yan. The policy-gradient placement and generative routing neural networks for chip design. *Advances in Neural Information Processing Systems*, 35:26350–26362, 2022.

Chien-Hsiung Chiou, Chin-Hao Chang, Szu-To Chen, and Yao-Wen Chang. Circular-contour-based obstacle-aware macro placement. In *2016 21st Asia and South Pacific Design Automation Conference (ASP-DAC)*, pp. 172–177. IEEE, 2016.

Zijie Geng, Jie Wang, Ziyan Liu, Siyuan Xu, Zhentao Tang, Mingxuan Yuan, HAO Jianye, Yongdong Zhang, and Feng Wu. Reinforcement learning within tree search for fast macro placement. In *Forty-first International Conference on Machine Learning*, 2024.

Jiaqi Gu, Zixuan Jiang, Yibo Lin, and David Z Pan. Dreamplace 3.0: Multi-electrostatics based robust vlsi placement with region constraints. In *Proceedings of the 39th International Conference on Computer-Aided Design*, pp. 1–9, 2020.

Shinn-Ying Ho, Shinn-Jang Ho, Yi-Kuang Lin, and WC-C Chu. An orthogonal simulated annealing algorithm for large floorplanning problems. *IEEE transactions on very large scale integration (VLSI) systems*, 12(8):874–877, 2004.

Tsung-Wei Huang and Martin DF Wong. Opentimer: A high-performance timing analysis tool. In *2015 IEEE/ACM International Conference on Computer-Aided Design (ICCAD)*, pp. 895–902. IEEE, 2015.

Andrew B Kahng, Sherief Reda, and Qinke Wang. Aplace: A general analytic placement framework. In *Proceedings of the 2005 international symposium on Physical design*, pp. 233–235, 2005.

Ateen Khatkhate, Chen Li, Ameya R Agnihotri, Mehmet C Yildiz, Satoshi Ono, Cheng-Kok Koh, and Patrick H Madden. Recursive bisection based mixed block placement. In *Proceedings of the 2004 international symposium on Physical design*, pp. 84–89, 2004.

Myung-Chul Kim and Igor L Markov. Complx: A competitive primal-dual lagrange optimization for global placement. In *Proceedings of the 49th Annual Design Automation Conference*, pp. 747–752, 2012.

Myung-Chul Kim, Natarajan Viswanathan, Charles J Alpert, Igor L Markov, and Shyam Ramji. Maple: Multilevel adaptive placement for mixed-size designs. In *Proceedings of the 2012 ACM international symposium on International Symposium on Physical Design*, pp. 193–200, 2012.

Myung-Chul Kim, Jin Hu, Jiajia Li, and Natarajan Viswanathan. Iccad-2015 cad contest in incremental timing-driven placement and benchmark suite. In *2015 IEEE/ACM International Conference on Computer-Aided Design (ICCAD)*, pp. 921–926. IEEE, 2015.

Scott Kirkpatrick, C Daniel Gelatt Jr, and Mario P Vecchi. Optimization by simulated annealing. *science*, 220(4598):671–680, 1983.

Yao Lai, Yao Mu, and Ping Luo. Maskplace: Fast chip placement via reinforced visual representation learning. *Advances in Neural Information Processing Systems*, 35:24019–24030, 2022.

Yao Lai, Jinxin Liu, Zhentao Tang, Bin Wang, Jianye Hao, and Ping Luo. Chipformer: Transferable chip placement via offline decision transformer. *arXiv preprint arXiv:2306.14744*, 2023.

Peiyu Liao, Siting Liu, Zhitang Chen, Wenlong Lv, Yibo Lin, and Bei Yu. Dreamplace 4.0: Timing-driven global placement with momentum-based net weighting. In *2022 Design, Automation & Test in Europe Conference & Exhibition (DATE)*, pp. 939–944. IEEE, 2022.

Yibo Lin, Shounak Dhar, Wuxi Li, Haoxing Ren, Brucek Khailany, and David Z Pan. Dreamplace: Deep learning toolkit-enabled gpu acceleration for modern vlsi placement. In *Proceedings of the 56th Annual Design Automation Conference 2019*, pp. 1–6, 2019.

Yibo Lin, David Z Pan, Haoxing Ren, and Brucek Khailany. Dreamplace 2.0: Open-source gpu-accelerated global and detailed placement for large-scale vlsi designs. In *2020 China Semiconductor Technology International Conference (CSTIC)*, pp. 1–4. IEEE, 2020.

Don MacMillen, Raul Camposano, D Hill, and Thomas W Williams. An industrial view of electronic design automation. *IEEE transactions on computer-aided design of integrated circuits and systems*, 19(12):1428–1448, 2000.

Igor L Markov, Jin Hu, and Myung-Chul Kim. Progress and challenges in vlsi placement research. In *Proceedings of the International Conference on Computer-Aided Design*, pp. 275–282, 2012.

Azalia Mirhoseini, Anna Goldie, Mustafa Yazgan, Joe Wenjie Jiang, Ebrahim Songhori, Shen Wang, Young-Joon Lee, Eric Johnson, Omkar Pathak, Azade Nazi, et al. A graph placement methodology for fast chip design. *Nature*, 594(7862):207–212, 2021.

Hiroshi Murata, Kunihiro Fujiyoshi, Shigetoshi Nakatake, and Yoji Kajitani. Rectangle-packing-based module placement. *Proceedings of IEEE International Conference on Computer Aided Design (ICCAD)*, pp. 472–479, 1995. URL `https://api.semanticscholar.org/CorpusID:13916081`.

Hiroshi Murata, Kunihiro Fujiyoshi, Shigetoshi Nakatake, and Yoji Kajitani. Vlsi module placement based on rectangle-packing by the sequence-pair. *IEEE Transactions on Computer-Aided Design of Integrated Circuits and Systems*, 15(12):1518–1524, 1996.

Gi-Joon Nam, Charles J Alpert, Paul Villarrubia, Bruce Winter, and Mehmet Yildiz. The ispd2005 placement contest and benchmark suite. In *Proceedings of the 2005 international symposium on Physical design*, pp. 216–220, 2005.

Jan M Rabaey, Anantha P Chandrakasan, and Borivoje Nikolic. *Digital integrated circuits*, volume 2. Prentice hall Englewood Cliffs, 2002.

Jarrod A Roy, Saurabh N Adya, David A Papa, and Igor L Markov. Min-cut floorplacement. *IEEE Transactions on Computer-Aided Design of Integrated Circuits and Systems*, 25(7):1313–1326, 2006.

Naveed A Sherwani. *Algorithms for VLSI physical design automation*. Springer Science & Business Media, 2012.

Yunqi Shi, Ke Xue, Lei Song, and Chao Qian. Macro placement by wire-mask-guided black-box optimization. In *Thirty-seventh Conference on Neural Information Processing Systems*, 2023.

M Shunmugathammal, C Christopher Columbus, and S Anand. A novel b* tree crossover-based simulated annealing algorithm for combinatorial optimization in vlsi fixed-outline floorplans. *Circuits, Systems, and Signal Processing*, 39:900–918, 2020.

Peter Spindler, Ulf Schlichtmann, and Frank M Johannes. Kraftwerk2—a fast force-directed quadratic placement approach using an accurate net model. *IEEE Transactions on Computer-Aided Design of Integrated Circuits and Systems*, 27(8):1398–1411, 2008.

Dhruv Vashisht, Harshit Rampal, Haiguang Liao, Yang Lu, Devika Shanbhag, Elias Fallon, and Levent Burak Kara. Placement in integrated circuits using cyclic reinforcement learning and simulated annealing. *arXiv preprint arXiv:2011.07577*, 2020.

Alex Vidal-Obiols, Jordi Cortadella, Jordi Petit, Marc Galceran-Oms, and Ferran Martorell. Rtl-aware dataflow-driven macro placement. In *2019 Design, Automation & Test in Europe Conference & Exhibition (DATE)*, pp. 186–191, 2019. doi: 10.23919/DATE.2019.8714812.

Alex Vidal-Obiols, Jordi Cortadella, Jordi Petit, Marc Galceran-Oms, and Ferran Martorell. Multilevel dataflow-driven macro placement guided by rtl structure and analytical methods. *IEEE Transactions on Computer-Aided Design of Integrated Circuits and Systems*, 40:2542–2555, 2021. URL `https://api.semanticscholar.org/CorpusID:232713780`.

Natarajan Viswanathan, Gi-Joon Nam, Charles J Alpert, Paul Villarrubia, Haoxing Ren, and Chris Chu. Rql: Global placement via relaxed quadratic spreading and linearization. In *Proceedings of the 44th annual Design Automation Conference*, pp. 453–458, 2007a.

Natarajan Viswanathan, Min Pan, and Chris Chu. Fastplace 3.0: A fast multilevel quadratic placement algorithm with placement congestion control. In *2007 Asia and South Pacific Design Automation Conference*, pp. 135–140. IEEE, 2007b.

Laung-Terng Wang, Yao-Wen Chang, and Kwang-Ting Tim Cheng. *Electronic design automation: synthesis, verification, and test*. Morgan Kaufmann, 2009.

Zhihai Wang, Zijie Geng, Zhaojie Tu, Jie Wang, Yuxi Qian, Zhexuan Xu, Ziyan Liu, Siyuan Xu, Zhentao Tang, Shixiong Kai, et al. Benchmarking end-to-end performance of ai-based chip placement algorithms. *arXiv preprint arXiv:2407.15026*, 2024.

A IMPLEMENTATION DETAILS

A.1 GRAPH REPRESENTATION

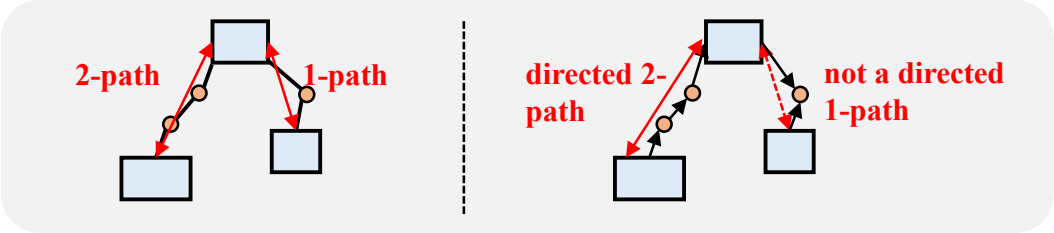

Figure 6: **Illustration of directed and undirected k-path.** The blue rectangles represent macros and orange dots represent cells. We mark the undirected and directed datapaths in two separate parts of the figure. In the right part, the connection directions are depicted with arrows.

We use a graph to represent each circuit. A circuit netlist often comprises hundreds of macros and numerous standard cells. We treat macros as nodes and capture the cell information as edge feature. We denote a path (which is connected by nets) consisting of k cells between two macros as a k-path, illustrated in Figure 6. For any two macros, notated as $node_i$ and $node_j$, the number of k-paths between them is denoted by $\mathcal{N}_{ij}^{(k)}$. We establish an edge between any two nodes, if there exists a path with depth not exceeding D between them. D represents the maximum depth of paths considered. The dataflow metric is used in EDA community to capture the "information closeness" between them (Vidal-Obiols et al., 2019; 2021). To capture the cell information, we introduce dataflow as our edge feature:

$$df_{i,j}^{(D)} = \sum_{1 \leq k \leq D} (\frac{1}{2})^k \cdot \mathcal{N}_{ij}^{(k)}, \tag{11}$$

Each net compromises both input and output components. Therefore, the connections between circuit modules are actually directed, analogous to the directed edges in a graph. Based on this, we introduce the concept of directed k'-path, as illustrated in Figure 6. We denote the number of directed k'-paths between $node_i$ and $node_j$ by $\mathcal{N}'^{(k')}_{ij}$. The corresponding directed dataflow $df'^{(D')}_{ij}$ can be calculated in the same way as Equation 11. We use both the directed and undirected cell connection information to establish the graph.

We formulate the circuit as a graph $\mathcal{G} = (\mathcal{V}_m, \mathcal{E}_{df})$. Here $\mathcal{V}_m \in \mathbb{R}^{\mathcal{N}_m \times d_m}$ and $\mathcal{E}_{df} \in \mathbb{R}^{\mathcal{N}_e \times d_e}$, where $\mathcal{N}_m$ and $\mathcal{N}_e$ refer to the number of macros and edges. d_m and d_e denote the number of feature channels for node and edge respectively. We assign three channels to our node feature $\mathcal{V}_m$, which are **physical information**: $size_x$ and $size_y$, namely the two-dimensional physical size of the macro; **logical information**: $npin$, namely the number of pins of the macro, which reflects the connected complexity of the macro. Based on the prior discussion, We assign a feature of $d_e = D + D' + 4$ channels to each edge. The edge feature of the $node_i$ and $node_j$ connection can be specifically denoted:

$$\mathcal{E}_{ij} = (df_{ij}^{(D)}, \mathcal{N}_{ij}^{(0)}, \cdots, \mathcal{N}_{ij}^{(D)}, df'^{(D')}_{ij}, \mathcal{N}'^{(0)}_{ij}, \cdots, \mathcal{N}'^{(D')}_{ij}). \tag{12}$$

In our work, we set D = 2 and D' = 10, obtaining a 16-channels edge feature.

A.2 L-MASK

As described in 2.3, LaMPlace aims to learn a L-mask for more general metrics of a chip circuit. In Appendix A.1, we have introduced the concept of dataflow, which is designed manually to quantify the connectivity properties between two macros. As shown in Equation 2, the coefficients $a_{i,j}^{(\lambda,k)}$ take a similar form with dataflow, which captures the pair-wise relationships between macros. Therefore, we refer to these coefficients as "learnable flows" (L-flows). Compared to dataflow, our learnable L-flows have Stronger representational capacity. Since L-flow is learned by predicting the cross-stage metrics, it can better correlate with the final chip quality.

L-mask is derived from L-flows. L-mask has a similar form with wiremask, namely, an $n \times n$ pixel-level feature map that represents the increase in the L-flow value if a macro is placed in a specific position. We detail the computation process for the L-mask in Algorithm 1. We also visualize the process of L-mask guiding placement in Figure 7.

Algorithm 1 Calculation of L-Mask

Input: Placed macros P, macro to be placed $macro_i$, L-flow $a_{i,j}^{(k,\lambda)}$
Parameters: Number of canvas partitions n, sum weight α_λ
Output: L-mask L
Initialize L as $n \times n$ grids of 0
for $macro_j$ **in** P **do**
  Get the grid position of $macro_j$, (x_j, y_j)
  Initialize G_x,G_y as $n \times n$ grids
  for $x \leftarrow 0$ to $n-1$ **do**
    for $y \leftarrow 0$ to $n-1$ **do**
      $G_x[x][y] \leftarrow x$
      $G_y[x][y] \leftarrow y$
  $R \leftarrow \sqrt{(G_x - x_j)^2 + (G_y - y_j)^2}$, quantifying the distance from grid cells to (x_j, y_j)
  $L \leftarrow L + \sum_\lambda \alpha_\lambda \sum_k a_{i,j}^{(k,\lambda)} \cdot R^k$
Return: The L-mask L

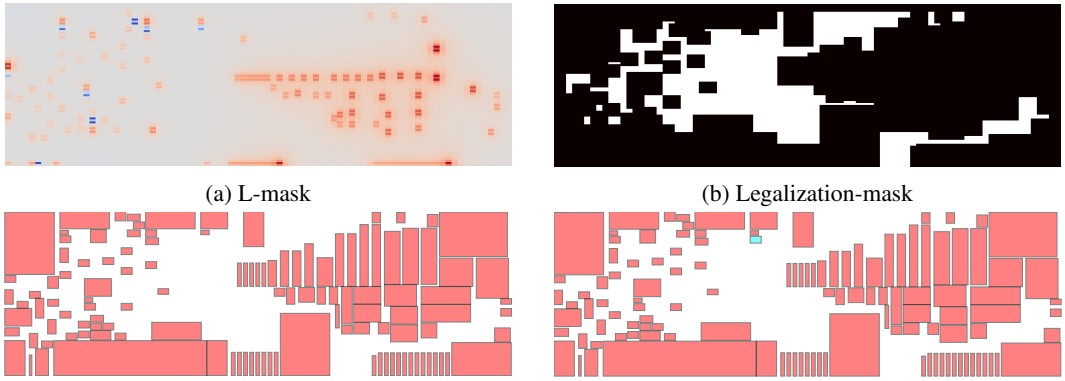

(a) L-mask (b) Legalization-mask (c) Pre-Placement (d) Step of Placement

Figure 7: **Illustration of L-mask guided macro placement.** In the L-mask figure (a), the blue pixels indicate the local minimum points. A legalization mask is applied to the L-mask to ensure no overlap. The white areas in Figure (b) indicates the legal positions for placement. Then, the legal position (no overlap) with the lowest L-mask value is selected for placing the next macro, which is represented by the blue macro in figure (d).

A.3 PLACEMENT ALGORITHM

We formulate the macro placement task as a black-box optimization problem. Evolutionary algorithm (EA) are employed where the genotype-phenotype mapping is greedily guided by L-mask. The random initial process records one best solution with the lowest predicted value and the following evolutionary process improves this solution by mutation. The mutation operator are implemented by randomly swapping the position of two macros. More algorithm details are demonstrated in Algorithm 2

Algorithm 2 Placement Algorithm

Input: Netlist $\mathcal{G} = (\mathcal{V}_m, \mathcal{E}_{df})$, L-flow $Lf_{i,j}^k$
Parameters: Number of initial random turns N_{init}, Number of evolutionary turns N_{ea}
Output: Placement P
For each $macro_i \in \mathcal{V}_m$, compute the connection weight of it, i.e., $\sum_{j,k} \left| Lf_{i,j}^k \right|$
Order all macros in decreasing order based on their connection weight, obtaining the ranked macro $\{macro_1^*, \cdots, macro_n^*\}$
for turns **in** N_{init} **do**
  Random initialize position for each $macro_i^*$, denoted by p_i
  Initialize placed-macros position as empty set, P
  Initialize best placement P^* with best value V^*
  for each $macro_i^*$ **do**
    Calculate the L-mask L_i based on placed-macros P and L-flow $Lf_{i,j}^k$ with the process in Algorithm 1
    $Q \leftarrow argminL_i$
    Select q from Q which is closest to the macro initial position p_i
    Incorporate $macro_i^*$ with position q to P
  Generate the predicted value V of final placement P
  if $V < V^*$ **then**
    $V^* \leftarrow V$
    $P^* \leftarrow P$
for turns **in** N_{ea} **do**
  Initialize position for each $macro_i^*$ as p_i^* from P^*
  Swap positions of two randomly selected macro
  Initialize placed-macros position as empty set, P
  for each $macro_i^*$ **do**
    Calculate the L-mask L_i based on placed-macros P and L-flow $Lf_{i,j}^k$ with the process in Algorithm 1
    $Q \leftarrow argminL_i$
    Select q from Q which is closest to the macro initial position p_i^*
    Incorporate $macro_i^*$ with position q to P
  Generate the predicted value V of final placement P
  if $V < V^*$ **then**
    $V^* \leftarrow V$
    $P^* \leftarrow P$
Return: The best placement P^*

A.4 BENCHMARK DETAILS

Table 2: **Statistics of public benchmark circuits.**

Circuit	Macros	Standard Cells	Nets	Pins	Area Util(%)
superblue1	424	1215820	1215710	3767494	85
superblue3	565	1219170	1224979	3905321	87
superblue4	300	801968	802513	2497940	90
superblue5	770	1090247	1100825	3246878	85
superblue7	441	1937699	1933945	6372094	90
superblue10	1629	984379	1898119	5560506	87
superblue16	99	985909	999902	3013268	85
superblue18	201	771845	771542	2559143	85

Table 2 details the statistics for eight circuits from the `ICCAD2015` dataset. Since larger modules generally exhibit greater complexity, modules larger than ten times the average area are selected as macros for placement. The "Macros" column specifies the quantity of macros chosen for placement in our study.

A.5 EXPERIMENTAL DETAILS

We report some important hyperparameters and settings in this section. Further details can be found in our code once the paper is accepted to be published. In our work, all the experiments are conducted on a single machine with NVidia GeForce GTX 3090 GPUs and Intel(R) Xeon(R) E5-2667 v4 CPUs 3.20GHz.

For the predictor training stage, we used DREAMPlace to generate 200 layouts and the corresponding metrics for each of six training circuits. This involved conducting 200 mixed-size placement runs for each circuit, each run using a different seed and the default settings. One fifth of the training set was selected as the validation set. We use the Adam optimizer to train our model for 400 epochs with a batch size of 60. We select the best model checkpoint based on the highest Kendall coefficient evaluated on the validation set. The Kendall coefficient is used to evaluates the ranking performance, as stated in (Chen et al., 2023). The learning rate is initialized to 0.001 and decays exponentially.

For the placement stage, since LaMPlace employs the same EA-search framework as WireMask-EA, which is thoroughly discussed in (Shi et al., 2023), we use the same configurations as WireMask-EA. The only difference lies in replacing the mHPWL-based WireMask with our L-mask. Both methods perform 50 random search iterations and 20 evolutionary iterations to obtain the final macro placement results. We fine-tune the pre-trained Chipformer model using its open-source code to generate macro placements for each test case. Since LaMPlace, Wiremask-EA and Chipformer all treat the chip canvas as a grid, as proposed in (Lai et al., 2022), we partition the grid into 84×84 across all the cases, aligning with (Lai et al., 2023). The evaluation of macro placement is conducted through cell placement using DREAMPlace and timing analysis with OpenTimer. In order to reduce the influence of randomness in a reasonable way, we pick five best macro placement layouts for each method and record the best evaluation result. For DREAMPlace, we obtain the mixed-size placement results with its default settings.

A.6 MODEL ARCHITECTURE AND HYPERPARAMETERS

We provide the structure and hyper-parameter details of our prediction model in this section. All the MLPs have two layers and use `ReLU()` as the activation function. We use the graph introduced in A.1 as our input. The details of the model hyper-parameter are shown in Table 3.
The input node and edge features are embedded using two MLP encoders. Next, multiple GNNs are employed to extract graph information, generating the node embeddings $\boldsymbol{h}_i$. After embedding $\boldsymbol{h}_i$ through the output encoder MLP, pairs of linear layers are used to obtain the Laurent polynomial coefficients between two nodes, as shown in Equation 2. Specifically, the message-passing process

Table 3: **Hyper-parameters of prediction model**

module	layer name	layer size	output size
edge encoder	MLP_1	16×256 `ReLU()` 256×256	(num of edges, 256)
node encoder	MLP_2	3×256 `ReLU()` 256×256	(num of nodes, 256)
graph encoder	GNN $\times 5$	256×256 for all MLPs	(num of nodes, 256)
ouput encoder	MLP_3	256×256 `ReLU()` 256×256	(num of nodes, 256)
L-flow decoder	Linear Layer $\times 16$	256×256 for all layers	(num of nodes, num of nodes, 16)

in a GNN can be represented by the following equations:

$$\begin{aligned} \boldsymbol{m}_{ij} &= \phi_e\left(contact(\boldsymbol{h}_i^{(l)}, \boldsymbol{e}_{ij})\right) \\ \boldsymbol{m}_i &= \sum_{j \in \mathcal{N}(i)} \boldsymbol{m}_{ji} \\ \boldsymbol{h}^{(l+1)} &= \phi_h(\boldsymbol{h}^{(l)} + \boldsymbol{m}_i), \end{aligned} \tag{13}$$

where $\mathcal{N}(i)$ is the neighbour of $node_i$, and ϕ_e, ϕ_h are non-linear mappings implemented by MLP.

A.7 Pair-wise Rank Loss

Learning to Rank is a machine learning framework that constructs a ranking model to optimize the correlation between predicted values and ground truth metrics. The pair-wise ranking method simplifies this problem into a binary classification task, focusing on distinguishing which candidate in a given pair is better. Given a pair of macro placement solutions, $< \mathbf{X}_i, \mathbf{X}_j >$, the predictor outputs their corresponding predicted metrics, $< \hat{y}_i, \hat{y}_j >$. If the true metrics satisfy $y_i > y_j$, denoted as $\mathbf{X}_i \succ \mathbf{X}_j$, the predicted probability of $\mathbf{X}_i$ being better than $\mathbf{X}_j$ is:

$$P(\mathbf{X}_i \succ \mathbf{X}_j) = \frac{1}{1 + exp\{-(\hat{y}_i - \hat{y}_j)\}}.$$

The rank loss for this pair is computed using a binary cross-entropy function, incorporating the difference caused by swapping the ranks of samples i and j:

$$L_{ij} = log\{1 + exp\{-(\hat{y}_i - \hat{y}_j)\}\}|\Delta Z_{ij}|,$$

where ΔZ_{ij} quantifies the difference in ranking caused by the swap, calculated using the softmax function:

$$\Delta Z_{ij} = \frac{exp(y_i)}{\sum_p exp(y_p)} - \frac{exp(y_j)}{\sum_p exp(y_p)}.$$

The total rank loss aggregates the pair-wise losses across all pairs and metrics:

$$L_{\text{Rank}} = \sum_{\lambda} \sum_{y^{(\lambda)}_{c_1,m_1} > y^{(\lambda)}_{c_2,m_2}} Z_{c_1,m_1,c_2,m_2} \log\left(1 + \exp\left(\hat{y}^{(\lambda)}_{c_2,m_2} - \hat{y}^{(\lambda)}_{c_1,m_1}\right)\right),$$

where λ denote each metric, and:

$$Z_{c_1,m_1,c_2,m_2} = \left| \frac{\exp\left(y^{(\lambda)}_{c_1,m_1}\right) - \exp\left(y^{(\lambda)}_{c_2,m_2}\right)}{\sum_{c,m} \exp\left(y^{(\lambda)}_{c,m}\right)} \right|.$$

This approach ensures that the ranking model effectively learns to prioritize solutions with higher metrics while considering the relative importance of each pair.

B ADDITIONAL RESULTS

B.1 RESULTS ON CHIPBENCH

We conduct experiments on ChiPBench Wang et al. (2024). We run the placement algorithm of LaMPlace directly on the industrial chips from ChiPBench without any fine-tuning, and follow their proposed workflow to obtain the final PPA metrics. The results are in Table 4. Notice that the baselines are tuned on the new dataset while our approach LaMPlace is not, demonstrating LaMPlace's zero-shot generalization ability.

Table 4: **Post-routing PPA results—Wirelength (um), Congestion, Power (W), WNS (ps), TNS (ps) and NVP—on ChiPBench.** For WNS and TNS, higher is better, and for other metrics, lower is better. Additionally, we report the average rank of these methods on each circuit. We mark the best results in **bold red**, and we mark the second best results in underline blue. LaMPlace achieves the best overall performance though baselines are tuned on the dataset while LaMPlace is not.

		swerv_wrapper	ariane133	bp_fe	bp	bp_be	ariane136
DREAMPlace	Wirelength	4525348	**6348638**	2823861	9347541	3518916	**6831531**
	Congestion	0.366	**0.2138**	0.5084	0.4088	0.5165	**0.2306**
	Power	0.645674	0.367289	**0.2942135**	0.2500424	0.458286	0.570734
	WNS	-1.06067	-0.540441	-1.11661	-2.10779	-2.16346	-1.35843
	TNS	-780.20	-690.27	**-473.261**	**-14.6088**	-3648.02	-3269.22
	NVP	1608	2307	1849	**192**	6026	4350
	Rank	2.29	2.00	2.14	**1.86**	3.00	2.14
WireMask-EA	Wirelength	4854661	6583143	2783740	10002159	3574875	6945252
	Congestion	0.41	0.23	0.51	0.44	0.52	0.24
	Power	0.67	0.37	0.31	0.25	0.47	0.57
	WNS	-1.02747	-0.417093	-1.66571	-1.93591	-2.14159	-1.72648
	TNS	-873.506	-329.353	-777.42	-21.8123	-4093.97	-4268.61
	NVP	1518	1970	2628	326	5131	3628
	Rank	2.71	2.86	3	3	3	2.286
Chipformer	Wirelength	5019849	6581086	2073376	**8970666**	3572070	6869186
	Congestion	0.43	0.23	0.38	**0.39**	0.52	0.24
	Power	0.67	0.37	0.30	**0.25**	0.43	0.57
	WNS	-1.19	-0.55	-1.20	-1.75	-2.17	-1.39
	TNS	-1282.24	-860.95	-1000.19	-502.98	-3541.82	-3603.53
	NVP	2139	2703	2714	2179	5100	3609
	Rank	2.67	2.50	3.17	3.00	3.33	3.33
LaMPlace	Wirelength	**4123153**	6947307	**1874385**	9840460	2854486	7051781
	Congestion	**0.35**	0.24	**0.34**	0.42	**0.41**	0.24
	Power	**0.636157**	**0.364683**	0.294396	0.257111	0.415	**0.545532**
	WNS	**-1.02**	**-0.19**	**-1.07**	**-1.73**	**-1.97**	**-1.13**
	TNS	**-740.69**	**-120.30**	-880.39	-53.47	**-2325.43**	**-2806.97**
	NVP	**1424**	**1533**	2676	400	4687	**3469**
	Rank	**1.00**	**2.00**	**1.83**	2.83	**1.00**	**2.00**

B.2 CASE STUDY ON PPA METRICS

We further evaluate those methods with the actual post-routing PPA metrics, using the Commercial Tool *Innovus*. The test metrics include routing wirelength (**rWL**), horizontal and vertical overflow (**rOverflowH** and **rOverflowV** respectively), post-routing timing metrics (**TNS**, **WNS**) and number of violations (**NVP**), i.e., the count of timing violation paths in a chip design. The detailed results are provided in Table 5, Table 6 and Table 7. Figure 8, Figure 9, and Figure 10 also provide the visualization of the final chip layouts. Figure 11 displays a histogram of the timing slack distribution for violated paths. Compared to other methods, the distribution for LaMPlace placements is more

concentrated near zero. These results demonstrate that LaMPlace significantly enhances the final PPA results compared with other tested methods.

Table 5: **Post-routing PPA results on superblue4, computed using *Innovus*.** We mark the best results in **bold red**.

	rWL($\times 10^8$um)	rOverflowH(%)	rOverflowV(%)	WNS(ps)	TNS($\times 10^5$ps)	NVP
DREAMPlace	2.15	71.62	46.67	-105.013	-4.47	45567
Wiremask-EA	1.90	70.90	19.40	-109.103	-2.69	22007
Chipformer	1.84	69.93	17.51	**-85.923**	-2.17	22627
LaMPlace	**1.53**	**9.93**	**0.32**	-87.170	**-1.77**	**13045**

Table 6: **Post-routing PPA results on superblue16, computed using Innovus.** We mark the best results in **bold red**.

	rWL($\times 10^8$um)	rOverflowH(%)	rOverflowV(%)	WNS(ps)	TNS($\times 10^5$ps)	NVP
WireMask-EA	1.13	9.21	0.15	-53.04	-2.12	21399
Chipformer	1.17	6.44	0.17	-91.19	-2.73	34606
DREAMPlace	1.41	16.31	1.66	-57.18	-1.90	30737
PolyMaP	**1.04**	**1.26**	**0.10**	**-45.06**	**-1.36**	**18776**

Table 7: **Post-routing PPA results on superblue18, computed using Innovus.** We mark the best results in **bold red**.

	rWL($\times 10^8$um)	rOverflowH(%)	rOverflowV(%)	WNS(ps)	TNS($\times 10^5$ps)	NVP
WireMask-EA	0.99	20.18	17.38	-61.63	-1.33	33151
Chipformer	0.95	18.41	12.44	**-50.227**	-0.64	17365
DREAMPlace	1.92	69.31	15.41	-65.014	-1.94	28477
PolyMaP	**0.95**	**9.48**	**5.79**	-88.967	**-0.51**	**11495**

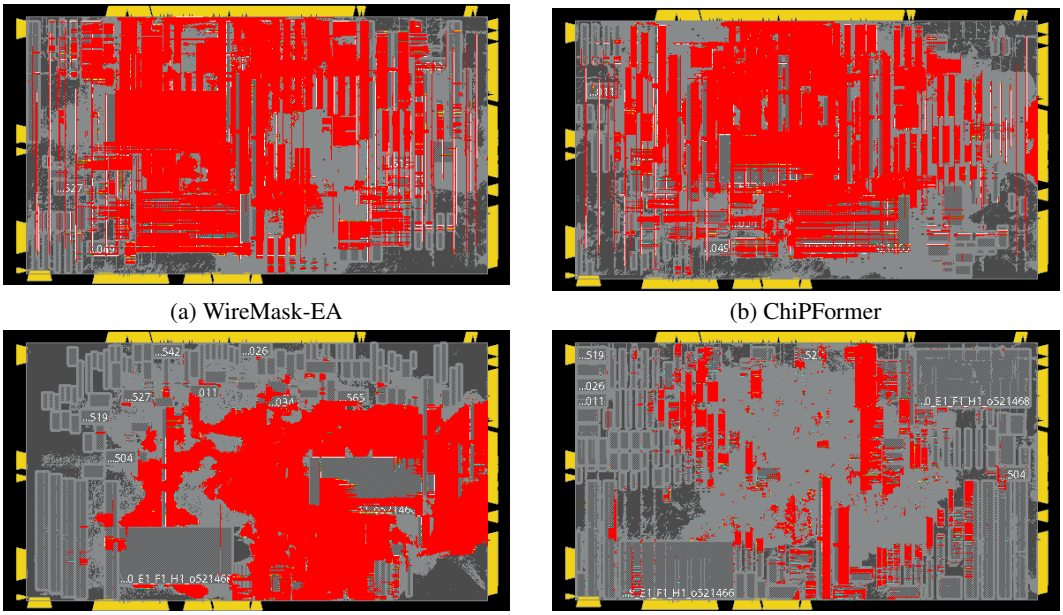

(a) WireMask-EA (b) ChiPFormer

(c) DREAMPlace (d) LaMPlace

Figure 8: **Visualization of post-routing results of *superblue4* using Commercial Tool *Innovus*.** The red area denotes the overflow area.

(a) WireMask-EA

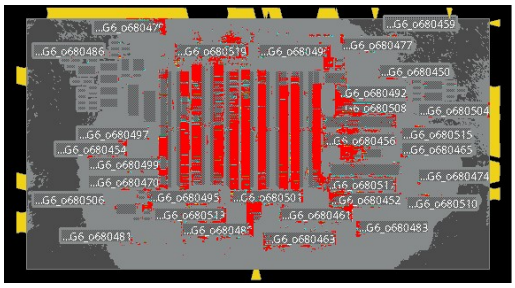

(b) ChiPFormer

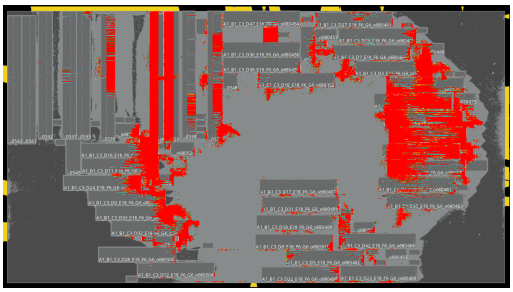

(c) DREAMPlace

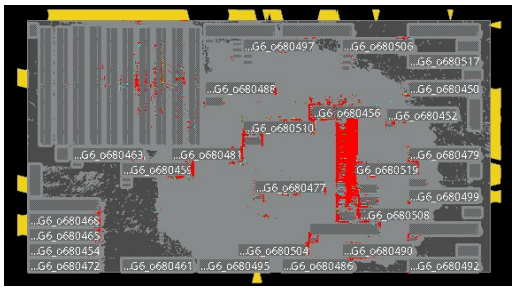

(d) LaMPlace

Figure 9: **Visualization of post-routing results of *superblue16* using Commercial Tool *Innovus***. The red area denotes the overflow area.

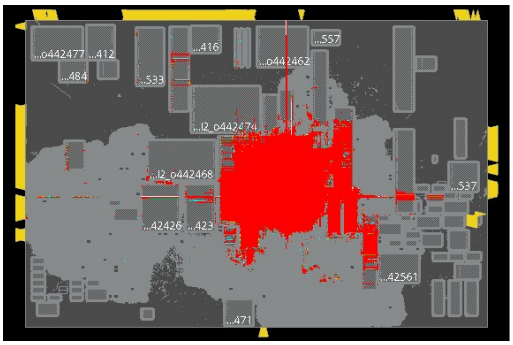

(a) WireMask-EA

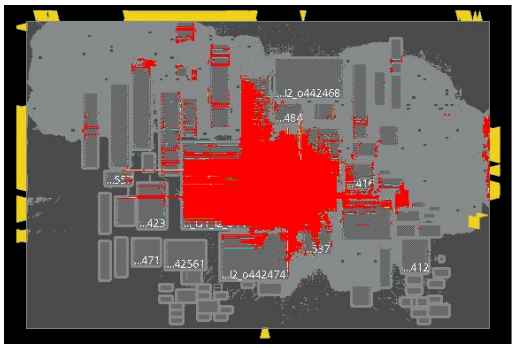

(b) ChiPFormer

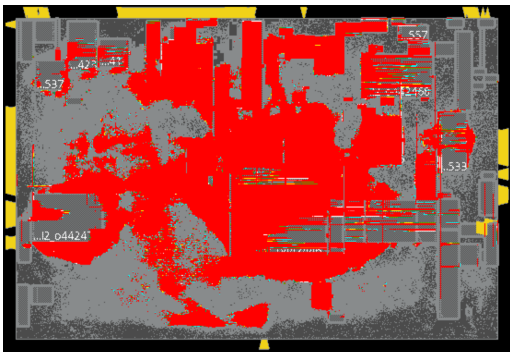

(c) DREAMPlace

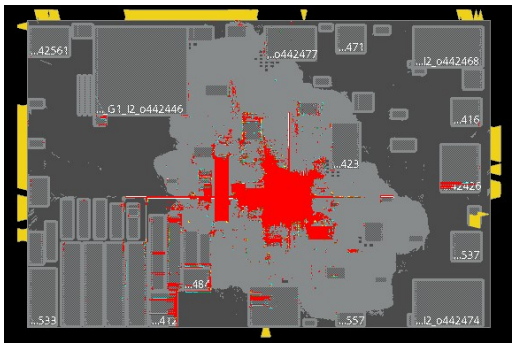

(d) LaMPlace

Figure 10: **Visualization of post-routing results of *superblue18* using Commercial Tool *Innovus***. The red area denotes the overflow area.

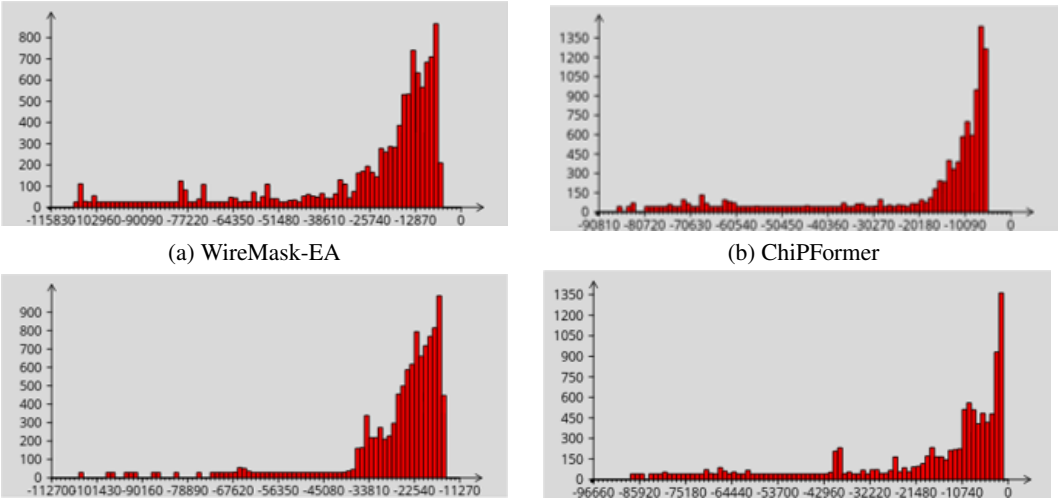

(a) WireMask-EA (b) ChiPFormer

(c) DREAMPlace (d) LaMPlace

Figure 11: **Histogram of post-routing timing slack results** of *superblue4* using Commercial Tool *Innovus*. The x-axis denotes the timing slack, while the y-axis quantifies the count of paths falling within specified timing slack intervals

B.3 Comparison Study on K

Table 8 presents the results of different choices of K, which is defined in Equation 1. The experiments are conducted with the same settings as the main experiments, expect for the different choices of K. According to the results, we empirically set $K = \{1, 0, -1, -2\}$ in the main experiments.

Table 8: Comparisons of HPWL ($\times 3.8 \times 10^{11}$ um), Cong. ($\times 10^{-2}$), TNS ($\times 10^{5}$ps), and WNS ($\times 10^{3}$ps) for macro placement derived by LaMPlace under different choices of K.

K		superblue1	superblue3	superblue4	superblue5	superblue7	superblue10	superblue16	superblue18
$\{1, 0, -1, -2\}$	HPWL	49.17	22.25	4.47	31.48	3.22	22.13	7.61	16.94
	Cong.	1.51	2.34	1.54	1.54	0.87	1.06	2.03	0.74
	TNS	-2422.01	-1797.7	-1424.31	-2889.21	-1585.32	7613.01	-1514.73	-426.91
	WNS	-127.31	-174.94	-84.01	-178.18	-66.02	-224.34	-36.87	-66.93
$\{0, -1, -2\}$	HPWL	31.05	18.44	6.61	20.61	4.49	20.59	6.22	4.99
	Cong.	1.62	2.41	1.64	1.523	1.31	0.99	2.05	0.78
	TNS	-3510.3152	-2157.98	-1764.7	-2541.66	-1249.57	-7203.3	-941.28	-378.25
	WNS	-167.51	-381.78	-104.92	-193.68	-51.11	-235.91	-30.89	-69.61
$\{2, 1, 0, -1, -2\}$	HPWL	55.53	27.11	8.69	69.01	3.5	25.32	7.59	8.46
	Cong.	1.8	2.5	1.85	1.98	1.67	1.25	2.12	0.87
	TNS	-1834.42	-1839.52	-1713.99	-3637.1	-1311.24	-7866.22	-1487.49	-375.03
	WNS	-140.41	-185.5	-108.25	-164.98	-47.65	-292.77	-33.96	-50.09
$\{1, 0, -2\}$	HPWL	38.08	21.57	8.07	45.29	4.99	11.6	6.93	28.47
	Cong.	1.63	2.47	1.58	1.36	1.17	1.02	2.06	0.83
	TNS	-3510.32	-2496.02	-1481.85	-2363.5	-1702.37	-8591.41	-1294.61	-250.23
	WNS	-167.51	-402.34	-84.96	-152.54	-66.42	-394.28	-36.36	-73.41

B.4 Comparison Study on $\{\alpha_\lambda\}_{\lambda \in \Lambda}$

We further study how the coefficients $\{\alpha_\lambda\}_{\lambda \in \Lambda}$ affect the placement results. To this end, we adjust $\{\alpha_\lambda\}_{\lambda \in \Lambda}$ to emphasize each of the metrics on the circuit *superblue4*. The results show that adjusting the hyperparameters can effectively control the final placement results. In main experiments, we simply set $\alpha_\lambda = 1$ for all λ.

Table 9: **Results of different weights of metrics.** Here the four coefficients correspond to HPWL, Cong., TNS, and WNS, respectively. The results are obtained on *superblue4*. We highlight the **best** result for each metric in bold, which aligns with our coefficients modification.

$\{\alpha_\lambda\}_{\lambda\in\Lambda}$	HPWL	Cong.	TNS	WNS
$\{1,1,1,1\}$	5.47	1.63	-1763.62	-123.71
$\{1,1,1,5\}$	4.734	1.47	-1708.66	**-81.45**
$\{1,1,5,1\}$	7.28	1.71	**-1579.60**	-90.47
$\{1,5,1,1\}$	4.35	**1.41**	-1880.33	-84.07
$\{5,1,1,1\}$	**1.83**	1.45	-1606.05	-99.03

B.5 Comparison Study on GNN Layers

We conduct an additional ablation study on the number of layers in the GNN architecture. The results are shown in Figure 12, demonstrating that the model performance is overall robust against the GNN architecture.

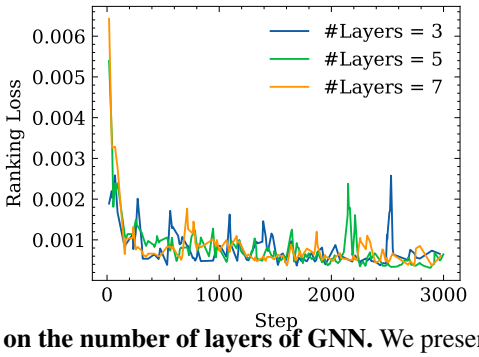

Figure 12: **Ablation study on the number of layers of GNN.** We present the training curves of the ranking loss with different GNN layers. The results are robust against the model architecture.

B.6 Runtime Analysis

We report the running time of the compared methods in Table 10. Both LaMPlace and Wiremask-EA undergo 50 initial turns followed by 20 evolutionary turns. The runtime for Chipformer is derived from fine-tuning a pre-trained model, while DREAMPlace conducts a mixed-size placement.

Table 10: **Running time(h) of compared methods to obtain the placement results.**

	superblue1	superblue3	superblue4	superblue5	superblue7	superblue10	superblue16	superblue18
DREAMPlace	0.28	0.25	0.14	0.34	0.46	0.47	0.20	0.18
Wiremask-EA	0.15	0.34	0.15	0.46	0.25	1.28	0.05	0.15
Chipformer	0.95	0.02	0.35	2.09	1.43	1.44	0.17	0.07
LaMPlace	0.22	0.38	0.11	0.72	0.21	3.16	0.01	0.05

B.7 Analysis on Training Loss

We analyze the correlation between the placement quality and the prediction error. The results are shown in Figure 13. The results demonstrate the positive correlation between the placement quality and the prediction error, while the placement quality is overall robust against the variations. We also present the training curves of several key metrics regarding the prediction error in Figure 14.

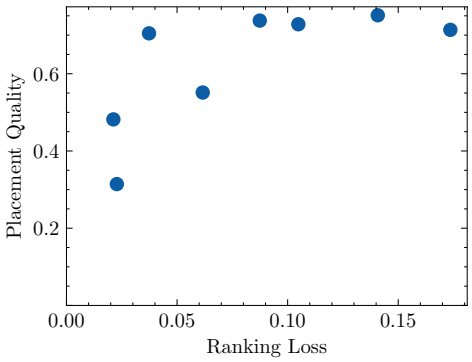

Figure 13: **The correlation between placement quality and prediction error.** We use models from 8 different checkpoints to compute ranking loss and perform macro placement on superblue16. The placement quality is evaluated by the average normalized values of the four considered metrics, lower indicating better. The results show that placement quality positively correlates with ranking loss, but it is still robust against variations.

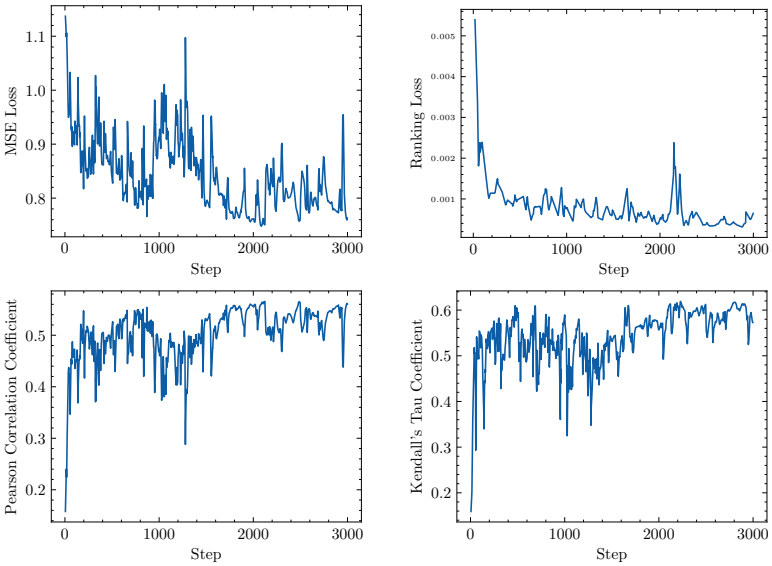

Figure 14: **Training curves of several key metrics regarding the prediction error.** The metrics include MSE loss, pair-wise ranking loss, Pearson and Kendall's Tau correlation coefficient. The results are computed on the validation set.

B.8 Visualization of Placement

We include the visualized results of DREAMPlace, WireMask-EA, Chipformer and LaMPlace in Figure 18, 16, 17 and 15. The visualizations highlight the distinct placement patterns of different methods. ChipFormer and WireMask-EA often place macros irregularly toward the center. DREAMPlace places macros and cells densely in the central area, optimizing HPWL but leading

to suboptimal PPA. In contrast, LaMPlace learns to place macros near edges or corners. From the perspective of an expert designer, this is usually a preferred practice as it benefits the back-end processes.

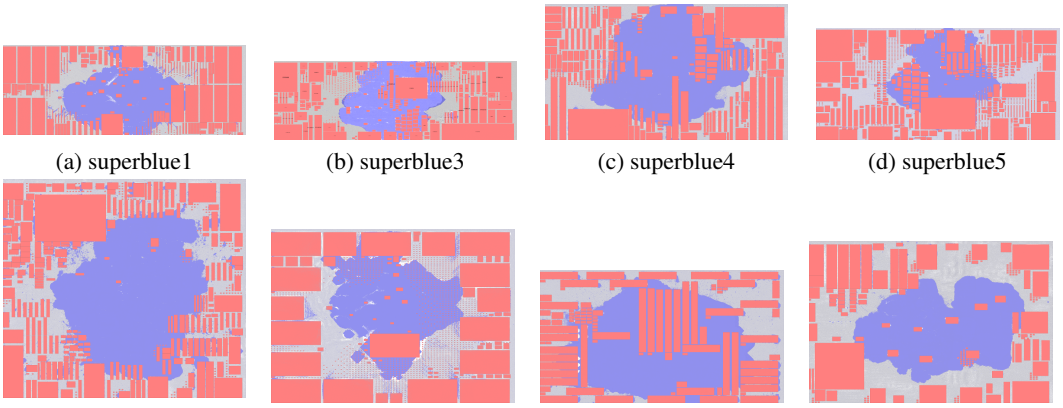

(a) superblue1 (b) superblue3 (c) superblue4 (d) superblue5

(e) superblue7 (f) superblue10 (g) superblue16 (h) superblue18

Figure 15: **Visualization of full-netlist placement results of all circuits in ICCAD2015 using LaMPlace.** Macros are marked in red, while standard cells are represented in blue.

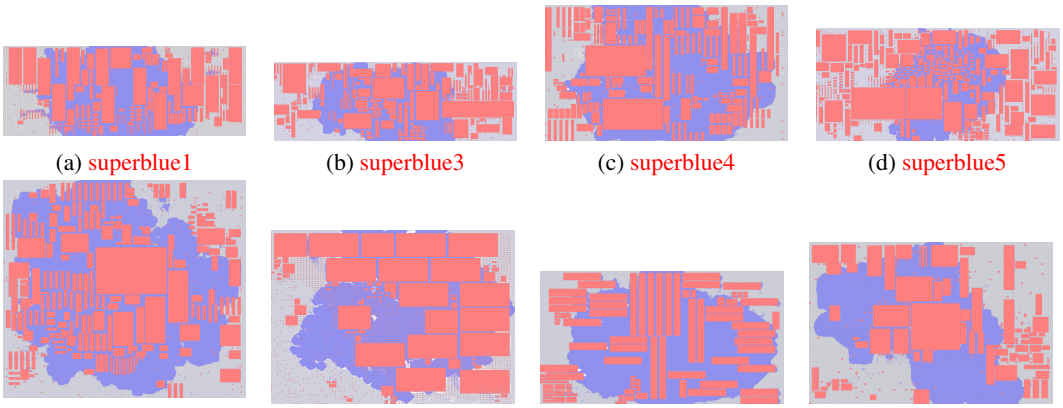

(a) superblue1 (b) superblue3 (c) superblue4 (d) superblue5

(e) superblue7 (f) superblue10 (g) superblue16 (h) superblue18

Figure 16: **Visualization of full-netlist placement results of all circuits in ICCAD2015 using WireMask-EA.** Macros are marked in red, while standard cells are represented in blue.

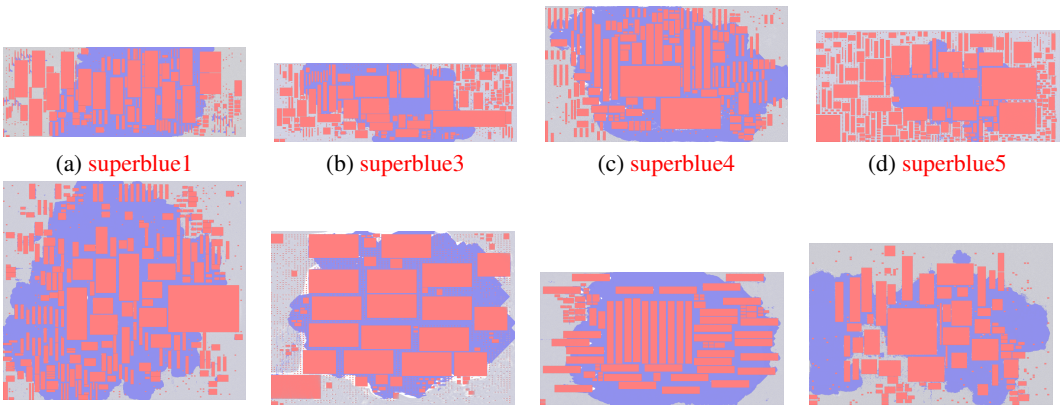

(a) superblue1 (b) superblue3 (c) superblue4 (d) superblue5

(e) superblue7 (f) superblue10 (g) superblue16 (h) superblue18

Figure 17: **Visualization of full-netlist placement results of all circuits in ICCAD2015 using Chipformer.** Macros are marked in red, while standard cells are represented in blue.

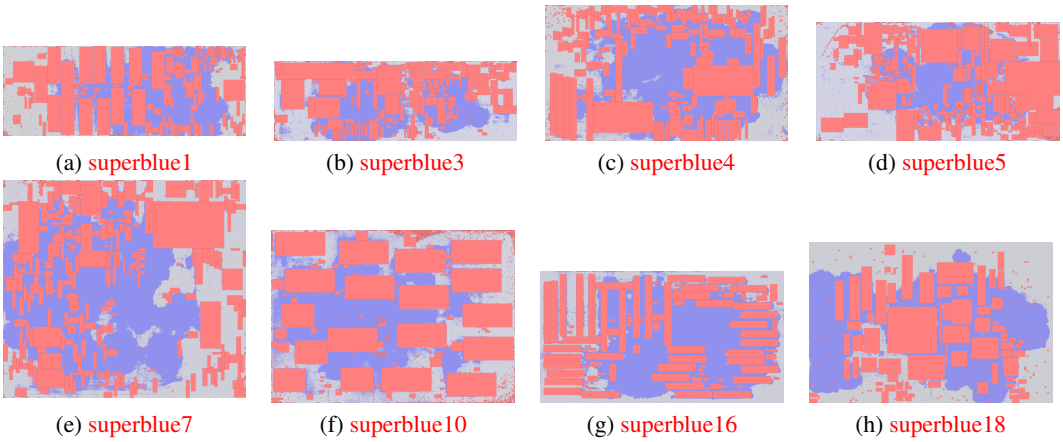

(a) superblue1 (b) superblue3 (c) superblue4 (d) superblue5

(e) superblue7 (f) superblue10 (g) superblue16 (h) superblue18

Figure 18: **Visualization of full-netlist placement results of all circuits in ICCAD2015 using DREAMPlace. Macros are marked in red, while standard cells are represented in blue.**

B.9 DREAMPLACE RESULTS DISABLING TIMING-DRIVEN OPTION.

We disable the timing-driven option in DREAMPlace, and evaluate timing results using OpenTimer. The results are included in Table

Table 11: Evaluation Results—HPWL ($\times 3.8 \times 10^{11}$um), Cong. ($\times 10^{-2}$), TNS ($\times 10^{5}$ps), and WNS ($\times 10^{3}$ps)—for DREAMPlace(mixed-size with timing-driven disabled)

	superblue1	**superblue3**	**superblue4**	**superblue5**	**superblue7**	**superblue10**	**superblue16**	**superblue18**
HPWL	22.8	26.5	8.2	29.02	20.76	1.81	10.5	7.29
Overflow	2.29	1.89	2.26	2.36	1.43	1.43	2.16	1.92
TNS	-6888.7	-2659.75	-1640.86	-11715.85	-4233.2	-3243.64	-2235.03	-445.23
WNS	-236.96	-327.83	-70.9	-362.18	-248.36	-268.71	-103.83	-73.2

B.10 ABLATION ON TRAINING DATASET

We conduct an ablation study to evaluate the impact of different sizes of the offline training dataset. In the manuscript, we use offline data from circuits superblue1, 3, 4, 5, 7, and 10 for training. For this ablation study, we train our model using the following subsets of circuits: (1) superblue1 and 3, and (2) superblue1, 3, 4, and 5. We provide the placement evaluation results for each ablation setting in Table 12. The results demonstrate the robustness of our method to varying amounts of training data. Also, it demonstrates using a larger training dataset shows some improvement in generalization performance (better placement for superblue16, 18).

Table 12: **Comparisons of HPWL($\times 3.8 \times 10^{11}$ um), Cong. ($\times 10^{-2}$), TNS ($\times 10^{5}$ps), and WNS ($\times 10^{3}$ps) with different training data sizes**

Train on two circuits	**superblue1**	**superblue3**	**superblue4**	**superblue5**	**superblue7**	**superblue10**	**superblue16**	**superblue18**
HPWL	52.26	13.65	5.31	29.89	2.48	23.41	6.48	14.06
Overflow	1.39	2.28	1.16	1.284	0.89	0.92	2.03	0.89
TNS	-2126.91	-1460.06	-1868.52	-2561.76	-2122.93	-8652.82	-1420.65	-586.32
WNS	-123.28	-212.67	-108.27	-165.59	-61.64	-266.42	-37.97	-71.44
Train on four circuits	**superblue1**	**superblue3**	**superblue4**	**superblue5**	**superblue7**	**superblue10**	**superblue16**	**superblue18**
HPWL	44.29	16.58	6.54	46.54	3.21	16.71	6.63	33.78
Overflow	1.47	2.29	1.08	1.01	0.83	1.01	1.99	0.74
TNS	-1965.85	-1882.6	-1671.95	-2659.65	-978.51	-8944.52	-1751.44	-275.91
WNS	-134.71	-230.69	-77.99	-156.55	-60.16	-324.07	-46.02	-49.01
Train on six circuits	**superblue1**	**superblue3**	**superblue4**	**superblue5**	**superblue7**	**superblue10**	**superblue16**	**superblue18**
HPWL	52.36	18.38	3.6	34.55	3.41	23.16	5.07	29.84
Overflow	1.43	2.39	1.21	1.39	0.79	0.98	2.08	0.75
TNS	-2020.33	-1456.38	-1338.81	-2719.28	-1160.47	-7339.67	-983.83	-335.66
WNS	-128.37	-220.89	-78.29	-160.61	-79.15	-193.11	-35.66	-49.09

C DISCUSSIONS

The increasing availability of large datasets in industrial environments highlights the potential of offline training for AI-driven placement optimization. In large EDA companies, where substantial chip data has already been accumulated, the focus is shifting toward leveraging existing datasets rather than repeatedly collecting new online data. This trend underscores the feasibility and effectiveness of offline pre-training approaches, such as the one proposed in this work, for modern placement tasks.

Our method demonstrates remarkable data efficiency and generalization capabilities. With a relatively modest dataset of 1,200 placement datapoints derived from open-source circuits, the model achieves strong performance across unseen chip designs. This modest computational demand for offline pretraining positions our approach as both practical and scalable. In contrast, prior reinforcement learning (RL)-based methods often necessitate thousands of online training steps, significantly increasing computational overhead and resource requirements.

Future research directions include exploring innovative data augmentation strategies to further enhance generalization. While directly perturbing chip layouts may inadvertently alter PPA metrics, alternative strategies, such as generating placement solutions using diverse placement methods or augmenting the dataset with more open-source netlists, hold promise. However, these strategies can be time-intensive and require further investigation. Expanding the dataset and refining augmentation methods are priorities for future work, aiming to strengthen the applicability and robustness of offline-trained models in diverse design environments.